University of Alberta

RUGGED CONTROL CIRCUIT FOR EFFICIENT OPERATION OF A WIND TURBINE

by

Glenn Edward Peters

A thesis submitted to the Faculty of Graduate Studies and Research in partial fulfillment of the requirements for the degree of **Master of Science**.

Department of Electrical Engineering

Edmonton, Alberta

Spring 2003

National Library of Canada
Acquisitions and Bibliographic Services
395 Wellington Street
Ottawa ON K1A 0N4
Canada

Bibliothèque nationale du Canada
Acquisitions et services bibliographiques
395, rue Wellington
Ottawa ON K1A 0N4
Canada

Your file Votre référence

Our file Notre référence

The author has granted a non-exclusive licence allowing the National Library of Canada to reproduce, loan, distribute or sell copies of this thesis in microform, paper or electronic formats.

L'auteur a accordé une licence non exclusive permettant à la Bibliothèque nationale du Canada de reproduire, prêter, distribuer ou vendre des copies de cette thèse sous la forme de microfiche/film, de reproduction sur papier ou sur format électronique.

The author retains ownership of the copyright in this thesis. Neither the thesis nor substantial extracts from it may be printed or otherwise reproduced without the author's permission.

L'auteur conserve la propriété du droit d'auteur qui protège cette thèse. Ni la thèse ni des extraits substantiels de celle-ci ne doivent être imprimés ou autrement reproduits sans son autorisation.

0-612-82328-8

Canada

University of Alberta

Library Release Form

Name of Author: Glenn Edward Peters

Title of Thesis: RUGGED CONTROL CIRCUIT FOR EFFICIENT OPERATION OF A WIND TURBINE

Degree: Master of Science

Year this Degree Granted: 2003

Permission is hereby granted to the University of Alberta Library to reproduce single copies of this thesis and to lend or sell such copies for private, scholarly or scientific research purposes only.

The author reserves all other publication and other rights in association with the copyright in the thesis, and except as herein before provided, neither the thesis nor any substantial portion thereof may be printed or otherwise reproduced in any material form whatever without the author's prior written permission.

Glenn Peters

Glenn Edward Peters
Box 21 Site 468 RR4
Sherwood Park, Alberta
Canada, T8A 3K4

Date: January 23, 2003

University of Alberta

Faculty of Graduate Studies and Research

The undersigned certify that they have read, and recommend to the Faculty of Graduate Studies and Research for acceptance, a thesis entitled **RUGGED CONTROL CIRCUIT FOR EFFICIENT OPERATION OF A WIND TURBINE** submitted by Glenn Edward Peters in partial fulfillment of the requirements for the degree of **Master of Science**.

Andrew M Knight

Dr. A. M. Knight
Supervisor

John Salmon

Dr. J. C. Salmon

Dr. E. P. Nowicki

Date: 22nd January 2003

Abstract

Wind is a viable energy source for remote loads where connection to a power grid is not practical. For a significant number of locations, the average wind speed is low and high system efficiency is very important. Unfortunately, batteries are commonly used for energy storage and the direct connection of a wind generator to a fixed DC voltage compromises the efficiency at low wind speeds. This research proposes a rugged wind energy controller that improves efficiency while keeping complexity to a minimum. The controller uses a boost DC-DC converter, a back-up module and fault detection circuitry. The wind energy controller has been verified in simulation and experimental testing. The simulation was performed in Matlab, modeling a wind turbine and AC generator charging a DC link via a diode bridge rectifier. Experimentally, the proposed converter was tested with a DC motor, an AC generator, a diode bridge and a DC load.

Acknowledgements

I would first of all like to give credit to Jesus Christ, my creator and the one who ultimately made this thesis possible.

Dr. Knight has been an excellent supervisor and has made this project a remarkably positive experience. He has exhibited patience, understanding and encouragement. I could not have had a better supervisor.

Dr. Salmon played a significant role in this research, freely offering his wealth of knowledge and experience.

My parents, grandparents and brothers have been a continual source of encouragement. They have taken a sincere interest in this work and have been more than willing to read my papers, listen to my ideas and give advice. Derek Peters deserves special recognition for his work in researching and providing specialized motors and equipment.

I am very thankful for my friends in the power lab, Ahmed Abasiry, Sergio Bertani and Albert Terheide, who have been more than willing to give me a hand when I needed it.

I am grateful to have been surrounded by so many fine individuals. I have truly been blessed.

Contents

1 Introduction 1

2 Wind Energy Principles 3

2.1 Meteorology 3

2.2 General Topology of a Stand-Alone, Small-Scale Wind Energy System 5

2.2.1 Wind Turbine 5

2.2.2 Electric Generators 6

2.2.3 Energy Storage 9

2.3 Speed Control of Wind Turbines 10

2.3.1 Speed Control Technology 10

2.3.2 Speed Control Schemes 10

2.4 Summary 11

3 Small-Scale Wind Energy Systems 12

3.1 Small-scale Wind Energy Systems For Charging Batteries 12

3.1.1 Problems With a Typical System 12

3.1.2 Possible Solutions 13

3.1.3 Circuit Topologies 14

3.1.4 Control Methods 15

3.2 Proposed System 17

3.2.1 Chosen Topology for a Small-Scale Wind System 17

3.2.2 Topology for a Fault Tolerant Converter 18

3.2.3 Control Method 19

3.3 Summary 20

4 Simulation **22**

4.1 System Parameters 22

4.2 Calculation of Ideal Relationship 23

4.3 System Simulation 25

4.3.1 Simulation Algorithm 25

4.3.2 Simulated Ideal Relationship 28

4.3.3 Dynamic Simulation Results 29

4.3.4 Effect of Changing the DC Offset in the Control Relationship 32

4.4 Fault Detection Circuit Simulation 34

5 Experimental Design **38**

5.1 Wind Turbine Simulator 39

5.1.1 DC Motor 39

5.1.2 Encoder 39

5.1.3 DC Current Controller 40

5.1.4 LabView Computer Control 41

5.2 Brushless Permanent Magnet Generator 43

5.3 DC Load 43

5.4 Proposed Controller 44

5.4.1 Boost Converter 44

5.4.2 Circuitry to Implement the Proposed Control Scheme 45

5.4.3 Fault Detection Circuit 46

5.4.4 Control Logic 46

5.5 Summary 49

6 Experimental Results **50**

6.1 Control Scheme 50

6.1.1 Verification of the Ideal Relationship 50

6.1.2 Proposed Control Scheme With a Dynamic Wind Speed . . . 51

6.2 Fault Tolerance Scheme 59

7 Conclusions and Future Work **62**

Bibliography **64**

List of Figures

2.1 Typical Topology of a Small-Scale, Stand-Alone System 5
2.2 Typical Turbine Performance Curve 6
2.3 Shunt Wound DC Generator Electrical Diagram 7
2.4 Induction Generator Electrical Diagram 8

3.1 Battery Charging Profile 13
3.2 Three Common DC-DC Converters 15
3.3 Control Topology 18
3.4 Turbine Torque 20

4.1 Algorithm for Finding the Ideal Relationship Between ω_e and V_{DC} . . 23
4.2 Ideal Terminal Voltage and Rotational Speed 24
4.3 Ideal Terminal Voltage Versus Rotational Speed 25
4.4 Simulation Algorithm 26
4.5 Generator Charging a Battery via a Diode Bridge Rectifier 27
4.6 Simplified Battery Charging Diagram 27
4.7 Simulated Ideal Relationship 29
4.8 Simulation Results With a Fixed DC link Voltage of 36 V 30
4.9 Simulation Results With the Proposed Control 31
4.10 Comparison of Simulated Energy and Power Capture 32
4.11 Results for a DC Offset of 8 V 33
4.12 Results for a DC Offset of 12 V 33
4.13 "Fault-Closed", Fault Detection Circuit 34
4.14 "Fault-Opened", Fault Detection Circuit 35
4.15 "Fault-Opened" Simulation Circuit 36

4.16 "Fault-Closed" Simulation Circuit 36
4.17 "Fault-Opened" Timing Capacitor Voltage 37
4.18 "Fault-Closed" Timing Capacitor Voltage 37

5.1 Experimental Test Rig Overview 38
5.2 DC Current Controller 40
5.3 Hysteresis Controller 41
5.4 DC Motor Control Algorithm 42
5.5 DC Load 44
5.6 Proposed Controller 45
5.7 Control Scheme Circuit 45
5.8 Fault Detection Circuit 47
5.9 Control Logic 48

6.1 Comparison of Optimal Control Relationships 51
6.2 Optimal Power Capture 52
6.3 Dynamic System Results with a Constant DC Link (36 V) 53
6.4 Power Capture for a Constant DC Link (36 V) 53
6.5 DC Link Voltage in the Uncontrolled Case 54
6.6 Uncontrolled and Ideal DC Link Voltages 54
6.7 Dynamic System Results with the Proposed Control 56
6.8 Power Capture with the Proposed Control 56
6.9 Comparison of Experimental Power and Energy Capture 57
6.10 Control Relationship 58
6.11 Fault Detection Scheme - Faulted Closed 60
6.12 Fault Detection Scheme - Faulted Open 61

List of Tables

2.1 Average Wind Speeds in Alberta (in m/s) 4

4.1 Simulation Parameters 22

5.1 DC Machine Specifications 39
5.2 DC Motor Torque-Current Relationship 40
5.3 Brushless Permanent Magnet Generator Specifications 43

6.1 Discontinuous Conduction Calculation Data 59

List of Symbols

A	wind turbine swept area
C	capacitance
C_p	coefficient of performance
D	damping
E	generator internal voltage
E_{diff}	largest induced voltage difference between machine phases
E_a, E_b, E_c	induced voltages in the a, b, c machine phases
I	current
I_{DC}	current in the DC link
I_{iB}	boost converter input boundary current
i	instantaneous current
J	inertia
K	machine constant
K_1, K_2	calculation constant
K_e	machine voltage constant
K_t	machine torque constant
L	inductance
P	power
R	resistance
R_1, X_1	stator resistance
R_2, X_2	Rotor Impedances
r	turbine radius
s	slip
T	torque

TSR	tip speed ratio
t	time
V	voltage
V_{Batt}	battery voltage
V_{DC}	DC voltage constant at the output of the diode bridge
V_{diff}	effective voltage across machine impedances
V_f	diode voltage drop
v_w	wind speed
X	reactance
x	length of an arbitrary section of moving air
δ	duty cycle
θ	electrical angular position
ϕ	flux density
ρ	density of air
τ	electrical time constant
ω_e	electrical frequency
ω_m	mechanical rotational frequency

Chapter 1

Introduction

Worldwide, wind is one of the fastest growing sources of electrical energy. During the 1990's, wind energy grew at annual rates between 25 percent and 35 percent [1]. Today the total installed wind energy capacity is more than 24,900 megawatts and is predicted to grow by 16 percent a year until 2006 [2]. The growth of wind energy is due, in part, to its ability to aid both social and economic goals. Socially, there are ever increasing environmental regulations imposed by national and international agreements (such as the Kyoto protocol). Economically, wind energy has become one of the most competitive forms of renewable energy generation with an estimated cost per kilowatt-hour of 4.0 to 6.0 US cents [3]. It is expected to become even more economically competitive as technology improvements are made. Such improvements are seen in the design and construction of multi-megawatt wind turbines. For example, GE Wind Energy is currently testing a 3.6 megawatt turbine for offshore applications [4].

For remote applications, where the cost of electricity is significantly higher than in a central location, wind energy is a compelling option. Examples include remote villages in developing countries or settlements located far away from main power lines. In fact, a remote load only has to be a few miles from a main power line for stand-alone wind generation to be cost effective [5]. Furthermore, in many developing countries, small, distributed generation is preferable to large centralized generation [6]. Diesel generation is also used as a solution for some of these remote locations. However, diesel fuel needs to be transported and stored - both of which significantly

affect the cost effectiveness of this option [7] [8].

When stand-alone wind generation is used, it is often the primary source of power. As a result, efficiency and reliability of the system are two very important factors. A typical small-scale wind generation system, used for charging batteries, can be extremely inefficient. System efficiency varies with wind speed, reaching an optimal performance at one specific operating point. Improving power capture over a wider range of wind speeds can be very valuable. However, improvements in efficiency can often compromise reliability. Power electronic control of the output power can be used to improve the efficiency of a wind energy system. The additional electronics, however, create an additional point of failure. Any improvement in power capture is irrelevant if the additional components fail and bring the system efficiency to zero.

An ideal system would contain the efficiency enhancing components, but would be able to replace these components if they were to fail. Such a system would maintain the reliability of the original system, but would allow for the improved power capture. The system would have to continuously monitor the efficiency improving components and generate a fault signal in case of a failure. The fault signal could be used to switch out the faulted components and bring healthy ones on-line. A system like this could actually be more reliable than the original system since the fault condition could be communicated and prompt servicing could take place.

This research examines the design of a power electronic controller for a small wind generator that does not compromise reliability. In a typical wind energy system, an AC generator's terminals are tied to a fixed battery voltage via a diode bridge rectifier. The proposed controller uses a boost DC-DC converter in the DC link to provide control over the generator terminal voltage. The controller implements a fixed relationship between generator electrical frequency and terminal voltage. Under a fault condition, the controller is designed to detect its own failure, completely isolate the failed components and continue normal operation. Both experimental and simulation results demonstrate the advantages of using the proposed converter in a typical wind energy system.

Chapter 2

Wind Energy Principles

Conversion of wind energy to electric energy requires a carefully controlled interaction of meteorological, mechanical and electrical systems. A basic understanding of these three systems and how they interact in a wind energy system is an important stage in the design of any wind energy system. Outlined in this chapter are the important wind energy principles required in the design process.

2.1 Meteorology

Wind is created by complex atmospheric systems, affected, in part, by solar radiation, surface cooling, humidity and the rotation of the earth [9]. These winds vary a great deal across time and geographic region and even local land formations, such as hills and trees, play a critical role in the behavior of a wind resource. As a result, wind power potential will vary from location to location. Within the province of Alberta, a great variation in average wind speed between locations can be observed (Table 2.1 [10]). This makes it difficult for wind energy companies to serve a large business region without giving individual consideration of power potential of each wind turbine installation.

In order to determine the power capture of a wind turbine, the power available in the wind must first be quantified. By taking the time derivative of the kinetic energy for a moving section of air,

Table 2.1: Average Wind Speeds in Alberta (in m/s)

Month	Location				
	Brooks	Calgary	Cowley	Edmonton	Edson
January	3.80	4.47	5.45	3.80	2.41
February	3.62	4.38	5.32	3.89	2.73
March	4.02	4.42	5.23	3.93	3.17
April	3.98	5.10	5.14	4.56	3.40
May	4.20	5.05	4.92	4.56	3.22
June	3.93	4.74	4.96	4.02	3.04
July	3.53	4.16	4.47	3.40	2.86
August	3.53	4.02	4.34	3.31	2.68
September	3.80	4.50	4.65	3.93	2.91
October	4.11	4.56	5.41	3.98	2.73
November	3.75	4.34	5.72	3.75	2.55
December	3.84	4.47	6.39	3.71	2.41

$$Energy = \frac{1}{2}\rho A x v_w^2 \tag{2.1}$$

an expression for wind power is obtained.

$$P = \frac{1}{2}\rho A^2 v_w^3 \tag{2.2}$$

Notice that instantaneous power is related to instantaneous wind speed in a cubic relationship, demonstrating that even a small increase in wind speed will result in a great increase in power. The cubic relationship, however, implies that average wind speed will not necessarily correspond with average power. Consider two identical wind turbines placed in regions with equal values for average wind speed. Suppose that the first region has a highly variable wind speed, while in the second region, the wind speed barely varies from the average. Due to the cubic relationship of equation 2.2, the turbine in the first region will capture more energy than the turbine in the second region. Furthermore, while there is very little instantaneous power available at low wind speeds, low wind speeds tend to be more frequent and are, therefore, extremely

important [10]. Considerations of the atmospheric system - its expected extremes and historical averages - play an important role in the design and component sizing of a wind energy system. For example, wind turbines are frequently located in regions where the wind speeds can be high enough to mechanically or electrically destroy the system. As a result, the wind turbine should be carefully matched to the generator and high wind power limiting should be employed (ie. forcing an aerodynamic stall or feathering the turbine blades [11]).

2.2 General Topology of a Stand-Alone, Small-Scale Wind Energy System

A typical small-scale, stand-alone wind energy system is composed of a wind turbine, an electric generator and an electric load. The wind turbine captures wind energy and converts it into rotational mechanical energy. The mechanical energy is converted to electrical energy with the electric generator. The electric energy output supplies the electric load.

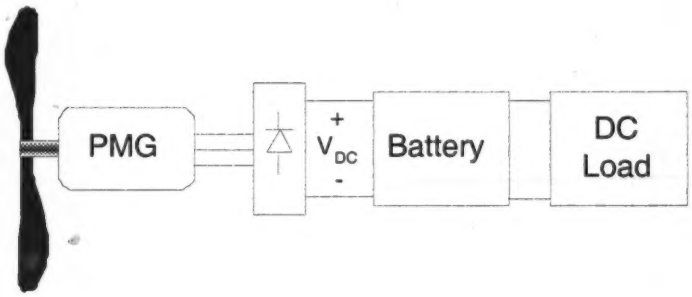

Figure 2.1: Typical Topology of a Small-Scale, Stand-Alone System

2.2.1 Wind Turbine

While wind turbines come in many forms, there are two main classes of wind turbines - those that rotate on a vertical axis and those that rotate on a horizontal axis. Wind turbines used for small-scale, stand-alone systems are usually made of two or three

blades and rotate on a horizontal axis. The property that most effectively describes the operation of a wind turbine is its Tip Speed Ratio (TSR).

$$TSR = \frac{r\omega_m}{v_w} \tag{2.3}$$

Turbine efficiency, known as the coefficient of performance (C_p), will vary with a wind turbine's TSR value and will reach a single maximum. Operation at or near the corresponding TSR value is necessary for efficient operation of a wind turbine. An optimal coefficient of performance is usually in the range of 0.3 to 0.4 [12], but has a theoretical maximum of 0.59, known as the Betz limit [9].

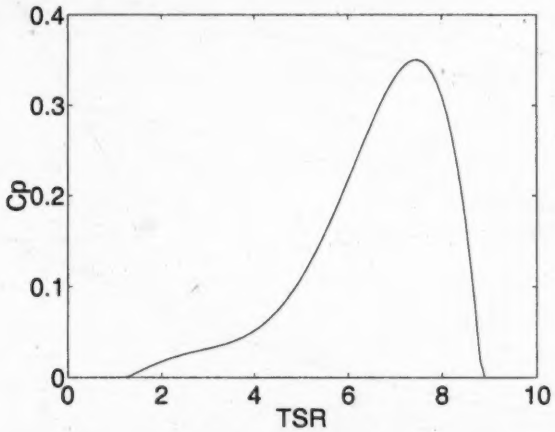

Figure 2.2: Typical Turbine Performance Curve

Figure 2.2 shows a typical plot of Cp versus TSR for a wind turbine. Notice that the optimum efficiency of the wind turbine occurs at only one TSR. In otherwords, for the most efficient turbine operation, the rotational speed of the wind turbine should change proportionally with wind speed. A system using a variable speed control will capture 20 to 30 percent more power than one using a fixed speed scheme. However, the increased energy capture comes at the cost of increased equipment and design complexity [13].

2.2.2 Electric Generators

Many types of electric generators have been successfully used in wind energy systems. The most common types of generators used for small-scale systems are the DC

generator, the Induction generator and the Brushless Permanent Magnet generator.

DC Generators

A DC generator is an obvious choice for stand alone systems, since batteries are often used for energy storage. In the 1930's, numerous farms across the prairies used wind energy for electricity and these wind systems almost exclusively used DC generators. The Jacobs wind turbine company, founded in the mid 1920's, was one of the main providers of wind energy systems at this time. Jacobs built very reliable DC Motor based wind systems - many of which are still in use today.

A DC generator is composed of a field winding and an armature winding. The field winding is wound onto the stator while the armature winding is wound onto the rotor and electrically connected to the external circuit by brushes and a commutator. In shunt wound DC machines, which are commonly used in wind energy systems, the field and armature windings are connected in parallel. Figure 2.3 demonstrates a typical electrical diagram for a system using a shunt wound DC generator and DC load [9]. The diode is used to prevent current from going from the battery to the DC machine. As the rotor spins, the armature windings cross the lines of flux set up by the field winding, inducing a voltage. The induced voltage, indicated by E in figure 2.3, forces current to the terminals.

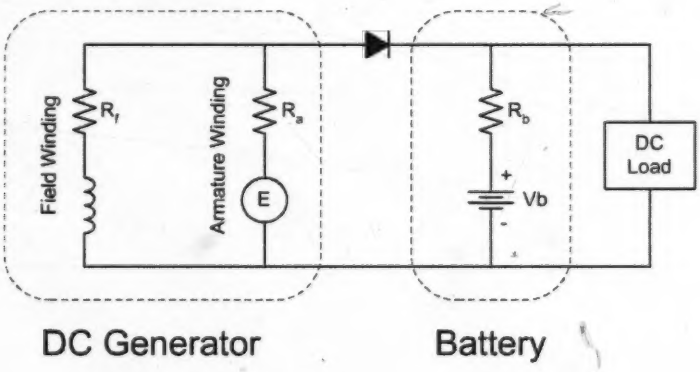

Figure 2.3: Shunt Wound DC Generator Electrical Diagram

Some DC machines use permanent magnets instead of a field winding. Permanent magnets maintain a constant field, while field windings require a continual excitation

current. A permanent magnet field is advantageous for small-scale, stand-alone systems, because the excitation current can use up a large percentage of the generated power - especially at low wind speeds.

Induction Generators

Induction generators are the most common type of electrical machine in today's industry. They do not use brushes, have a very simple and rugged construction and are cheap to produce. Induction generators incorporate a wound stator and a rotor that is usually built with iron laminations and an aluminum "squirrel cage". The iron laminations reduce eddy currents and thereby, reduce internal losses. The aluminum squirrel cage interacts with the stator windings to produce electricity. A simplified circuit diagram for an induction generator is shown in Figure 2.4 [9]. R_1 and X_1 are the stator impedances and R_2 and X_2 are the rotor impedances. X_m is the magnetizing reactance and R_m represents the losses due to eddy currents and hysteresis losses. All of the values are referred to the rotor.

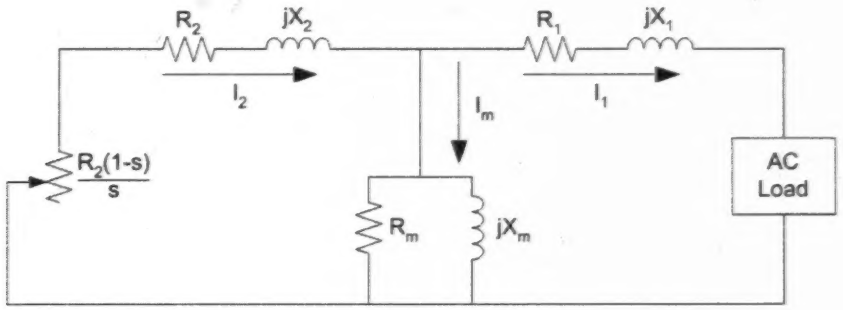

Figure 2.4: Induction Generator Electrical Diagram

The current through X_m is reactive must be specially supplied to the induction machine. If the induction machine is connected to a power grid, the reactive current can be obtained from the grid. For a stand-alone system, capacitors can be placed across the generator terminals to provide the reactive current. Since the capacitors will be ideally sized for a specific rotational speed, their usefulness over variable speeds will be limited. However, carefully sizing a series-parallel combination of capacitors at the generator terminals has been shown to work effectively over variable speeds

[14].

Brushless Permanent Magnet Generators

Brushless permanent magnet generators operate under a very simple principle - a principle similar to DC machines. A constant magnetic field is established and made to pass over windings. Every time a line of flux passes over a conductor, a voltage is induced (ie. Faraday's Law). The permanent magnets are placed on the rotor and the windings are placed on the stator.

The Brushless Permanent Magnet generator has a number of advantages over DC and induction machines. Like induction motors, they are very rugged, not requiring brush maintenance. Efficiency is improved as there are no I^2R losses in rotor or field conductors. Brushless permanent magnet generators, however, are more expensive than induction generators, but the increased cost is offset by a lack of a need for capacitors.

2.2.3 Energy Storage

Since wind is a constantly varying resource, it cannot be relied upon to give power all of the time. Energy usually needs to be stored so that, during times of low or no wind speed, power can continue to be delivered to the load. Batteries are the most common form of energy storage, though other forms such as flywheels [15] and hydrogen [16] are popular research topics [13]. There are cases where energy storage is not a requirement and an intermittent power is suitable. An example might be wind electric water pumping [17]. When the wind blows, water is pumped into a reservoir and when the wind is not blowing, the reservoir, acting indirectly as an energy storage device, can supply the needed water.

Currently, the use of batteries is the most effective way of storing electrical energy for small scale systems. Batteries have significant problems such as a limited charging rate, a limited life span and an intolerance to significant overcharging [13]. Proper battery charging can be accomplished with a charge controller which will take an input voltage, convert it to a proper battery charging voltage and possibly even ensure that the batteries do not overcharge by diverting the excess power to a dump

load (eg. resistive heating). Batteries recharge better with a steady charging current as opposed to sudden bursts of high current. For this reason, capturing wind energy, even in low wind speeds, is very important.

2.3 Speed Control of Wind Turbines

2.3.1 Speed Control Technology

Speed control of wind turbines has often been accomplished with pitchable turbine blades. The pitch is controlled with hydraulic and mechanical systems that allow the wind turbine to follow predefined operating conditions. A variable-pitch turbine, however, is significantly more expensive than a fixed-pitch turbine. As a result, variable-pitch turbines tend to be more common in large systems where the cost per unit of energy may be lower for the added expense.

Another method of control is the use of power electronics. The generator terminal voltage and current are controlled to bring the wind turbine into the desired operating conditions. Power electronic control has become more viable in recent years as the cost of power semiconductors has decreased. Unfortunately, it can introduce high frequency noise to the system and for systems which are grid connected, additional filtering is required to bring the power quality up to standard.

Many other technologies have been applied to wind energy systems to achieve speed control. They have included techniques such as pole changing in induction machines, gear changing between generator and turbine or even a Scherbius variable-speed drive. [13]

2.3.2 Speed Control Schemes

There are three basic methods for controlling the speed of a wind turbine - a fixed speed, a two speed and a variable speed scheme. As of 1997, 45 percent of all turbines used a two speed scheme, while 35 percent used a fixed speed scheme and 25 percent a variable speed scheme [18].

In a fixed speed scheme where the rotational speed of the wind turbine is controlled to be constant, turbine overspeeding is never a problem, but the turbine will rarely

operate at its highest efficiency. Referring to figure 2.2 and equation 2.3, if the rotational speed is held constant and the wind speed varies, then the wind turbine will be optimally efficient at one wind speed. With variable-pitch blades a turbine can operate at a good efficiency over a range of wind speeds [9], but as was mentioned in section 2.3.1, variable-pitch control adds significant expense to a system [19].

An improvement on the fixed speed scheme is the two speed scheme. In this case, the wind turbine operates at two different rotational speeds, based on wind speed. The two rotational speeds are chosen so that the ideal efficiency for each rotational speed occurs at wind speeds on either side of the average wind speed. This scheme can be implemented by changing the gear ratio between the turbine and generator or designing the generator to operate at two different speeds based on how the stator pole windings are connected. A higher number of stator poles would be used for the lower turbine speed and the lower number of poles for the higher turbine speed. [13]

In a variable speed scheme, the turbine can be controlled to follow a specific TSR or can be left uncontrolled. The advantages of the uncontrolled scheme are its simplicity and the low cost. For these reasons, the uncontrolled scheme is extremely common in small systems. The disadvantage is that this scheme will rarely perform at optimum efficiency.

A controlled variable speed scheme will achieve the highest overall efficiency of any system. This type of system has more "elasticity," reducing power and torque pulsations created by a fluctuating wind [20]. In these systems, pitch control may be used to reduce output power in high winds. Due to these advantages variable speed systems are becoming increasingly common [18].

2.4 Summary

Wind energy systems are composed of a wind turbine, an electrical generator and an electrical load. Each of these components must be sized and tuned to the local or typical meteorological conditions. Various control schemes can be used to improve system efficiency, but economic viability and reliability will determine their use.

Chapter 3

Small-Scale Wind Energy Systems

3.1 Small-scale Wind Energy Systems For Charging Batteries

Typically, modern wind generators create AC power and in small systems - especially ones used for charging batteries - power electronics are used to rectify the AC power to DC. This conversion may be accomplished with either a diode bridge rectifier or a fully controlled rectifier. The diode bridge rectifier is preferred due to its simplicity as there is no associated control circuitry or stressful hard switching of devices. While diode bridge rectification with a permanent magnet generator and battery load is very simple, there are significant associated problems. This section outlines some of these problems and some possible solutions.

3.1.1 Problems With a Typical System

When an AC generator supplies a DC load, via a diode bridge rectifier (figure 2.1), significant problems can occur in both high and low wind speed conditions. In low wind speeds, the generator may not rotate fast enough to induce a voltage to overcome the diode reverse bias produced by the DC link. In high wind speeds, the output power of the generator will be limited by an increased reactive impedance. [21] This is illustrated in figure 3.1, where a family of typical turbine power curves are shown for various wind speeds. Superimposed on these curves is the generator output power

which would result from a connection to a fixed DC load. The relationship between generator power and wind speed is given by the locus of intersection of these curves. Power limiting in high wind speeds can be useful for constraining turbine speeds [19] [22]. However, a reduced power capture in low wind speeds serves no useful purpose and reduces system efficiency.

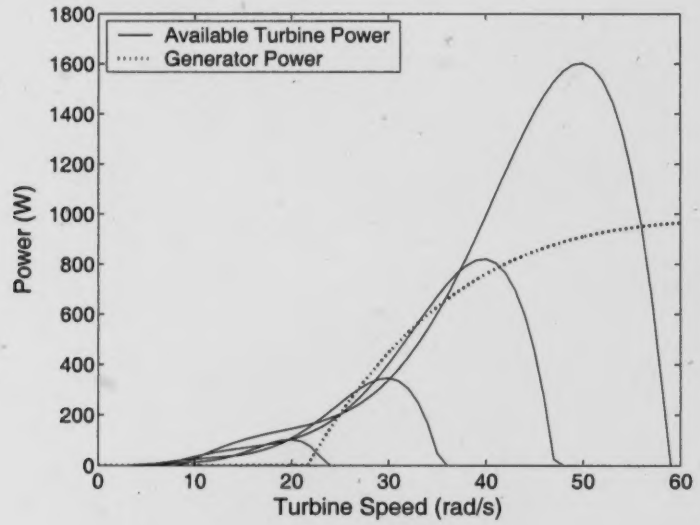

Figure 3.1: Battery Charging Profile

3.1.2 Possible Solutions

Between the high and low wind speed regions, there is a point where power transfer is very good. The most common solution to this problem is to ideally size the DC voltage (based on a typical wind profile) so that the most power is captured on an annual basis. Typically, the system is sized so that the maximum C_p is achieved at the rated power of the machine [22]. Power capture in low wind speeds is sacrificed for the overall system performance.

Another solution is series capacitor compensation [21]. Choosing a capacitor to resonate with the reactive impedance at high frequencies will reduce the equivalent impedance and increase the power capture in high wind speed regions. A drawback of this approach is that the natural generator current limiting is bypassed and rated

generator current can be exceeded. For this to be an effective method, special power limiting methods should be employed.

A DC-DC converter inserted between the diode bridge rectifier and DC load can control the impedance match between the generator and DC load. A DC-DC converter will control the DC voltage of the diode bridge rectifier, the generator terminal voltage and, thereby, the generator current. Since

$$T = K\phi I \tag{3.1}$$

controlling generator current will control generator torque and turbine speed. Therefore, by controlling the DC voltage, a high efficiency can be achieved at all wind speeds. In addition, at high wind speeds, the generator current will be naturally limited to a safe value - unlike series capacitor compensation.

3.1.3 Circuit Topologies

Several circuit topologies for the control of a small-scale wind system have been successfully implemented and tested by other researchers. Some have used a fully controlled AC to DC converter, while others have used a diode bridge rectifier accompanied with a DC-DC converter.

AC to DC converters are common in larger wind energy systems, but to achieve a precise and smooth AC to DC conversion, position sensors are needed to detect the phase of a synchronous generator. These sensors are relatively expensive for small systems (ie. less than 10 kW) [23], so use of a diode bridge rectifier with a DC-DC converter is preferred. Furthermore, the input power factor of a diode bridge rectifier is high and the use a DC-DC converter reduces the number of switches by a factor of six.

There are three common types of DC-DC converters - the buck, the boost, and the buck-boost (figure 3.2). The buck converter has been shown to work effectively [24], but is not commonly used. Wind turbines tend to spin at low speeds (ie. less than 1000 rpm) and produce low output voltages. A buck converter would reduce the voltage even more and transmission of power at low voltages increases I^2R losses.

A boost converter (which increases the DC link output voltage) helps to reduce I^2R losses - especially for installations where the DC power is transmitted over a long

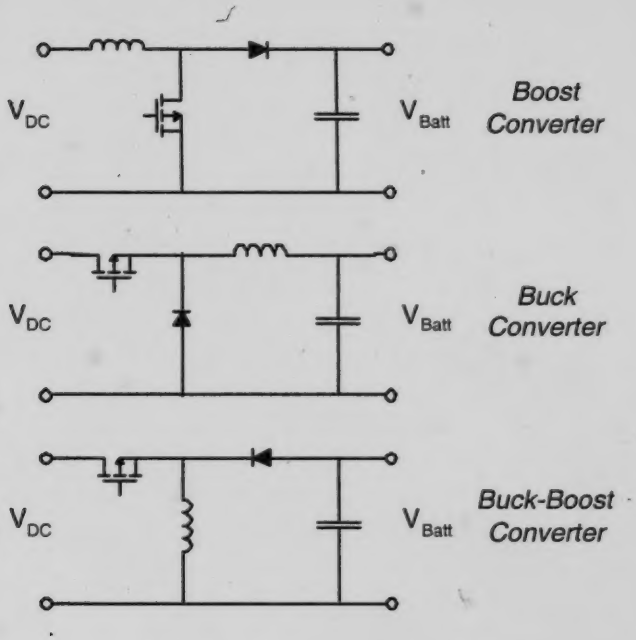

Figure 3.2: Three Common DC-DC Converters

distance. Since the boost converter eliminates the "cut-in" wind speed, the generator can be sized for larger powers (ie. the number of turns per pole can be reduced) [25]. This reduces the reactive losses at high frequencies. It is shown in the next chapter that the boost converter naturally lends itself to a fault tolerant scheme, keeping the redundant components to a minimum.

The buck-boost configuration has been successfully demonstrated in literature [23][26]. It both increases and decreases the generator terminal voltage, depending on what is needed.

3.1.4 Control Methods

Wind is a continuously changing resource and control of the electrical load on a wind generator is an extremely important issue. In order to maintain a high wind turbine efficiency, the turbine load should be varied in order to keep the turbine TSR relatively constant. An obvious method of achieving a constant TSR is to directly measure wind speed and calculate the desired rotational speed. The error between the actual rotational speed and the desired rotational speed is calculated and fed to

the control system. Unfortunately, accurate measurement of wind speed at the wind turbine is difficult due to the shadowing effects of the wind turbine on an anemometer [13]. Also, small changes in the surface of wind turbine blades can significantly affect the ideal TSR value. Therefore, the TSR set-point may have to be modified over the life of the wind turbine. Several other methods of control have been proposed which do not depend on a direct measurement of wind speed. Two general categories of control are systems using Maximum Power Point Tracking (MPPT) and systems using a fixed relationship control. In both, the electrical load is changed to bring the wind energy system to a more efficient operating point.

Maximum Power Point Tracking

For every wind speed, the relationship between turbine speed and power has a single peak. By increasing or decreasing the electrical load in small increments, the speed of the wind turbine can be changed. If an incremental change in electrical load causes an increase in power, the electrical load will be further increased until the maximum power is achieved. This form of control is known as Maximum Power Point Tracking (MPPT). It is insensitive to changes in system parameters or errors in wind speed measurements [13]. A drawback of this method of control is that it is necessary to search for the best operating characteristics every time the wind speed changes. Wind speeds can change rapidly, while turbines, which have a large inertia, change speed slowly. Yamamura et al. [23] and Schiemenze and Steibler [27] have demonstrated MPPT for a small wind energy system and a large wind energy system respectively. However, Bowmick and Spee [28] note that while the MPPT algorithm is simple, it can be slow. They propose using an MPPT algorithm to fine tune the system operating point and a heuristic model to estimate wind speed. The fine tuning accounts for small changes in system parameters while the heuristic model is used to speed up the control. While this scheme improves performance, it increases complexity.

Fixed Relationship Control

A common method of control involves measuring the speed of the wind generator as the feedback variable and controlling the electrical load to follow a fixed relationship

with the generator speed. Since wind turbine power is described by,

$$P = \frac{1}{2}\rho C_p A^2 v_w^3, \tag{3.2}$$

substitution of equation 2.3 for TSR gives a new equation for power.

$$P = \frac{1}{2}\rho C_p A^2 \frac{r^3}{TSR^3}\omega_m^3 \tag{3.3}$$

If the TSR is maintained at the optimum value, then the peak power versus rotational speed will follow a known cubic relationship. Since the ideal operating point is known ahead of time, the system does not have to search for it. Lawrance et al.[25], Venkataramanan et al.[22] and De Broe et al.[26] have used fixed relationships between output power versus wind speed or rotational speed to set the operating point. They have shown this to be an effective method of control.

3.2 Proposed System

As discussed in Chapter 1, the goal of this research is to design a power electronic controller that can ensure an efficient turbine operation while providing a fault tolerant topology. The proposed system uses a brushless permanent magnet generator, a diode bridge rectifier, a boost DC-DC converter and a battery load. The boost DC-DC converter is controlled to follow a fixed relationship between electrical frequency and generator terminal voltage. The control scheme is implemented with discrete analog components.

3.2.1 Chosen Topology for a Small-Scale Wind System

This research considers a typical small-scale wind system topology using a brushless permanent magnet generator supplying a DC load via diode bridge rectifier. A brushless permanent magnet generator was chosen for the reasons described in Chapter 2 (ie. ruggedness, simplicity and efficiency). The proposed system supplies a battery load and a boost DC-DC converter in the DC link provides control over the generator's terminal voltage. The boost DC-DC converter was chosen because it can be conveniently applied in a fault tolerant scheme and it provides a high voltage output which will reduce I^2R losses.

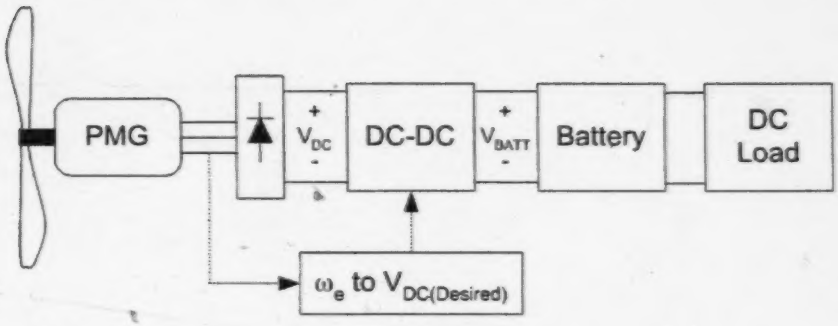

Figure 3.3: Control Topology

3.2.2 Topology for a Fault Tolerant Converter

A fault tolerant system should be able to detect when a failure has occurred and take remedial action. The system should be able to work around the faulted components or provide for a simple replacement of the faulted components. The parts requiring replacement should be kept to a minimum. Fortunately, a boost converter provides a topology that will help to keep component overhead to a minimum.

If a failure occurs in either the mosfet or diode (of the boost converter in figure 3.2), they can be replaced as a pair without having to replace any other components. Furthermore, the inductor and capacitor are located in places which conveniently compliment a wind energy system for battery charging. First, when the diode bridge conducts, the generator inductance contributes to the boost inductance (possibly eliminating the need for a boost inductor). Secondly, the battery is in parallel with the boost capacitor and helps to support the DC link voltage. This reduces the required capacitance since the capacitor is only needs to filter out the high frequency switching noise.

The fault detection circuit monitors the voltage across the primary switch and detects for either a switch or diode fault in the primary converter. In the event of a fault, the primary converter is switched out of the DC link using relays. The relays are dual pole and while switching out the primary converter, the backup converter will be switched into the DC link.

The proposed converter allows for control over the DC link voltage, but does not compromise reliability. In fact, the proposed converter could actually increase system

reliability. If remote sensing was used and a failure occurred in a remote, stand-alone wind energy system, the fault detection circuitry would detect an abnormal condition and generate a fault signal. The fault signal could be transmitted to a central location and immediate knowledge of a wind system failure would be known.

3.2.3 Control Method

In the proposed system, the wind speed does not need to be measured directly, but is determined from the electrical frequency of the generator voltage. Referring to Figure 3.3, the electrical frequency is deduced from the turbine rotational speed. Based on the turbine rotational speed, a reference mosfet duty cycle is generated to give the desired DC link voltage.

A fixed relationship between electrical frequency and DC link voltage is used since the ideal operating point can be determined ahead of time. In order to improve the system response to a wind gust, the fixed relationship is given a slightly positive DC offset. Since electrical frequency is used to control the terminal voltage of the generator, the control system will never actually know what the wind speed is at a given point in time. If the wind speed increases or decreases, the turbine torque will increase or decrease respectively, and the turbine speed will change. If the terminal voltage is set slightly above the ideal, then, compared to the optimal condition, the generator current will be slightly lower, the generator current will be slightly lower and, as a result, the turbine speed will be slightly higher. Referring to Figure 3.4, point "a" represents a situation where the turbine is operated at its most efficient point. If the wind speed increases from 8 ms^{-1} to 9 ms^{-1}, the system operating point will move to point "b". Conversely, point "c" represents a situation where the turbine is operated at just above the ideal speed. When the wind speed increases from 8 ms^{-1} to 9 ms^{-1}, the system operating point moves to point "d". Comparing these two situations, it can be seen that in moving from point "c" to "d", the system experiences a larger change in torque than in moving from point "a" to "b". Therefore, if the system experiences a larger change in torque when the wind speed increases, then according to

$$T_{Turbine} = T_{Generator} + J\frac{d\omega_m}{dt}, \tag{3.4}$$

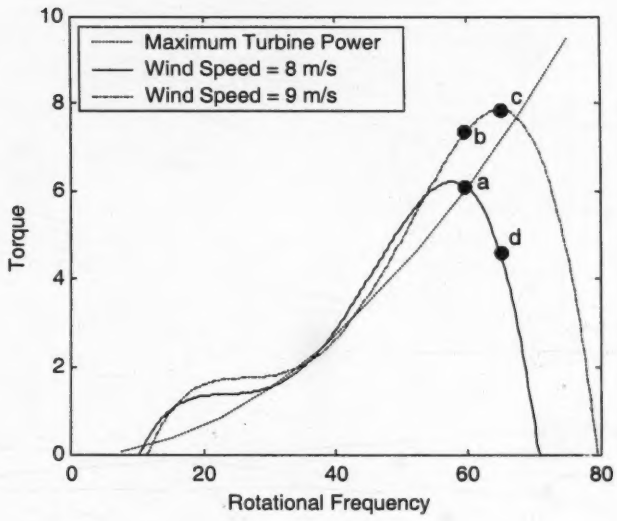

Figure 3.4: Turbine Torque

(which describes the torque balance between electric generator and wind turbine) the system will be able to accelerate more quickly to the next steady state operating point.

If the DC voltage is given a small positive offset above the ideal voltage, the diode bridge is not in danger of being reverse biased. The ideal terminal voltage will be well below the generator induced voltage limit for the majority of wind speeds. However, at low wind speeds, the commanded DC link voltage will be higher than the induced voltage limit of the generator. In this case, the DC link voltage will be held at the generator induced voltage limit, thereby creating a knee in the observed DC voltage versus electrical frequency relationship.

3.3 Summary

The proposed system will control the generator terminal voltage through the use of a boost DC-DC converter in the DC link. The introduction of fault detection circuitry should ensure reliable operation, switching out a faulted converter for a backup system if necessary. The proposed control scheme uses a fixed relationship between electrical

frequency and DC link voltage - not requiring MPPT or wind speed measurements. To verify the proposed design, the system is simulated and experimentally tested in Chapters 4 and 6 respectively. The detailed design is discussed in Chapter 5.

Chapter 4

Simulation

Outlined in this chapter are the simulation procedures and results for the proposed system. A straight line control relationship is developed and the proposed control procedure and fault detection circuitry are verified.

4.1 System Parameters

Simulation parameters are used to match those of the experimental test rig described in Chapter 5. The parameters are listed in Table 4.1.

Table 4.1: Simulation Parameters

Turbine Radius	1.0 m
Phase to Phase Winding Inductance	3.71 mH
Phase to Phase Winding Resistance	0.6 Ω
Peak Phase to Phase Voltage Constant	86 $V/kRPM$
Peak per Phase Torque Constant	0.71 Nm/A
Poles	8
System Inertia	1.2 $kg \cdot m^2$
System Damping	0.16 $Nm/kRPM$
Diode Bridge Forward Voltage Drop	1.0 V

4.2 Calculation of Ideal Relationship

Since the proposed control scheme follows a straight line relationship between electrical frequency and generator terminal voltage, a basic calculation demonstrating the validity of this approach is accomplished. Over a range of wind speeds, electrical frequency and steady state terminal voltage are calculated assuming an ideal TSR value and a unity power factor diode bridge. The calculation algorithm is outlined in figure 4.1.

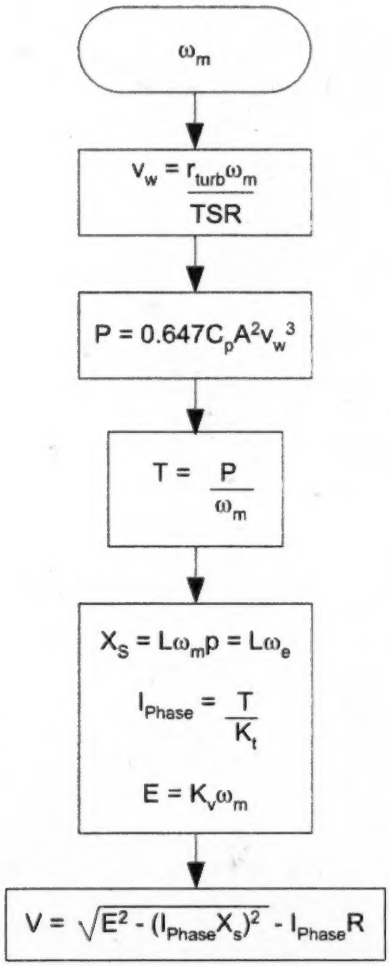
ω_m
$v_w = \frac{r_{turb}\omega_m}{TSR}$
$P = 0.647 C_p A^2 v_w^3$
$T = \frac{P}{\omega_m}$
$X_S = L\omega_m p = L\omega_e$
$I_{Phase} = \frac{T}{K_t}$
$E = K_v\omega_m$
$V = \sqrt{E^2 - (I_{Phase}X_s)^2} - I_{Phase}R$

Figure 4.1: Algorithm for Finding the Ideal Relationship Between ω_e and V_{DC}

Initially, using the turbine curve of figure 2.2, a set of turbine tip speeds and wind

speeds that achieve an ideal TSR (ie. TSR = 7.5) are calculated. Next, the turbine power corresponding to the wind speeds and an ideal C_p are evaluated. Based on the turbine power, the turbine torque can be determined. Finally, all the electrical quantities including reactive impedance, line current, electromotive force and line voltage are calculated.

The resulting DC voltages and mechanical frequencies are plotted against wind speed in figure 4.2. Note that there is a unique relationship between mechanical frequency and line voltage. In Figure 4.3, line voltage is plotted against electrical frequency. The relationship is linear for the majority of rotational speeds and exhibits a slightly negative concavity in the higher rotational speeds. As a result, for a system with the given parameters, a linear relationship should be an effective method of control. The linear relationship may begin to deviate from the ideal relationship in higher wind speeds and, in turn, compromise an optimal capture of wind energy. However, this may be a useful method of limiting the power capture in excessively high winds.

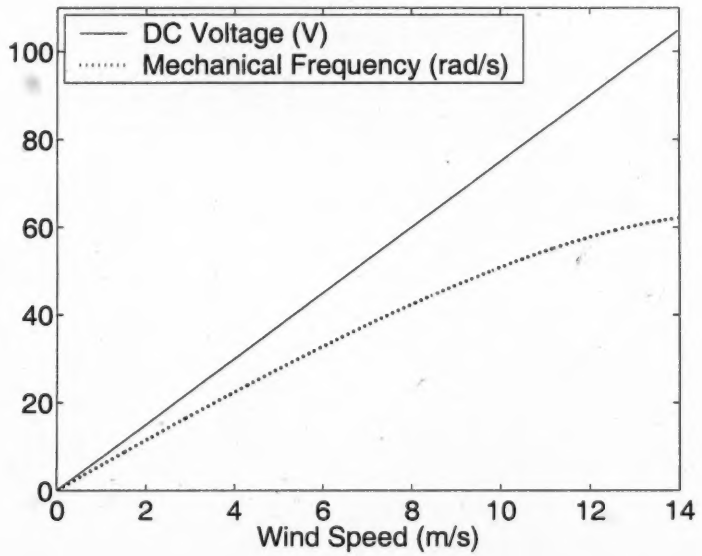

Figure 4.2: Ideal Terminal Voltage and Rotational Speed

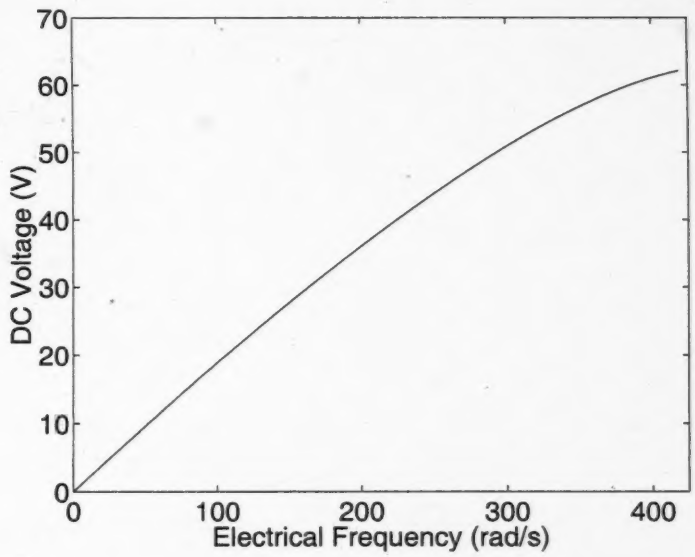

Figure 4.3: Ideal Terminal Voltage Versus Rotational Speed

4.3 System Simulation

The proposed control scheme was tested with a simulation that modeled the wind turbine, the brushless permanent magnet generator and a diode bridge rectifier. The output of the diode bridge rectifier was varied based on a voltage commanded by the control scheme. A DC-DC converter was not simulated at this point since the focus was on a proper control relationship between electrical frequency and DC link voltage.

4.3.1 Simulation Algorithm

The system was simulated in Matlab using a method similar to one used by Venkataramanan [22]. The simulation recursively evaluates the calculations outlined in figure 4.4. Based on the system parameters and an input wind speed, the turbine, generator and friction torques are evaluated. The net torque is used to calculate the rotational speed and, thereby, the generator induced voltage. The differences between the per-phase induced voltages are calculated and the greatest positive difference (E_{diff})

$$E_{diff} = Maximum \ | \ [(E_a, E_b, E_c) - (E_a, E_b, E_c)] \ | \tag{4.1}$$

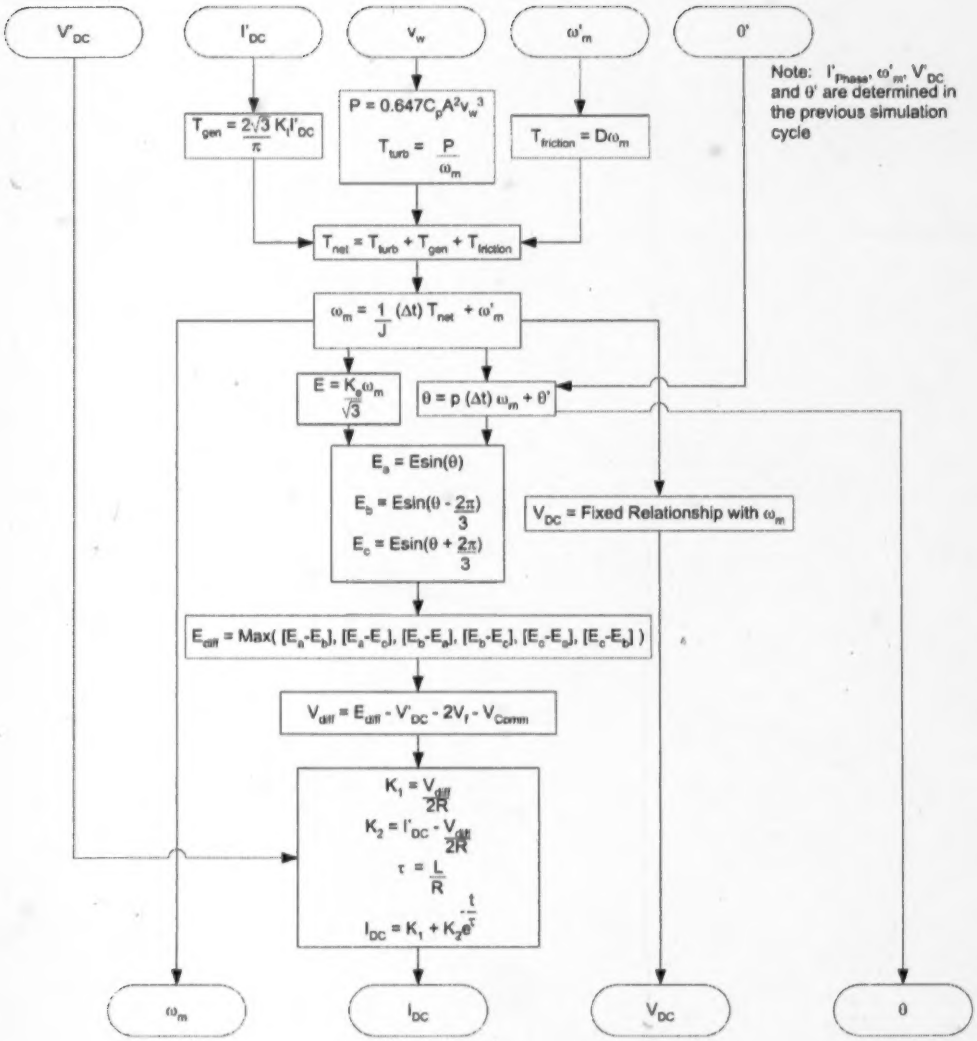
V'DC
I'DC
Vw
ω'm
θ'
Note: I'Phase, ω'm, V'DC and θ' are determined in the previous simulation cycle
Tgen = 2√3 / π KI I'DC
P = 0.647CpA²Vw³
Tturb = P / ωm
Tfriction = Dωm
Tnet = Tturb + Tgen + Tfriction
ωm = 1/J (Δt) Tnet + ω'm
E = Ke ωm / √3
θ = p (Δt) ωm + θ'
Ea = Esin(θ)
Eb = Esin(θ - 2π/3)
Ec = Esin(θ + 2π/3)
VDC = Fixed Relationship with ωm
Ediff = Max([Ea-Eb], [Ea-Ec], [Eb-Ea], [Eb-Ec], [Ec-Ea], [Ec-Eb])
Vdiff = Ediff - V'DC - 2Vf - VComm
K1 = Vdiff / 2R
K2 = I'DC - Vdiff / 2R
τ = L / R
IDC = K1 + K2 e^(-t/τ)
ωm
IDC
VDC
θ

Figure 4.4: Simulation Algorithm

is compared with a DC link voltage (which is set by the control scheme). If the DC link voltage is greater than E_{diff}, then the line current will be zero. Otherwise, the line current will be positive indicating conducting diodes.

The difference between E_{diff} and the DC link voltage is represented as V_{diff}. V_{diff} is used to calculate the line current and is calculated based on a voltage drop across two resistances, two inductances and two diodes (equation 4.2). The reason for a voltage drop across two impedances is because a conducting diode bridge rectifier will connect two of three generator phases. This is illustrated in Figure 4.5 and simplified in Figure 4.6. The effect of commutation overlap is also considered (equation 4.3), since this will have a significant effect at higher wind speeds.

$$V_{diff} = E_{diff} - 2V_f - V_{Comm} - V_{DC} \tag{4.2}$$

$$V_{Comm} = 6\frac{\omega_e}{2\pi}LI_{line} \tag{4.3}$$

The line current in figure 4.6 is time varying and can be described by equation 4.4.

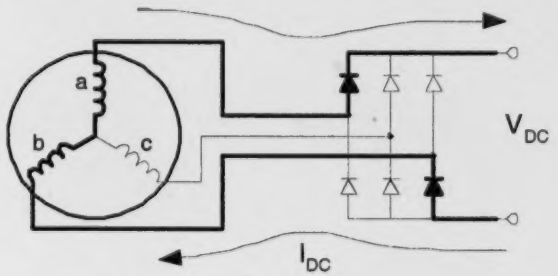

Figure 4.5: Generator Charging a Battery via a Diode Bridge Rectifier

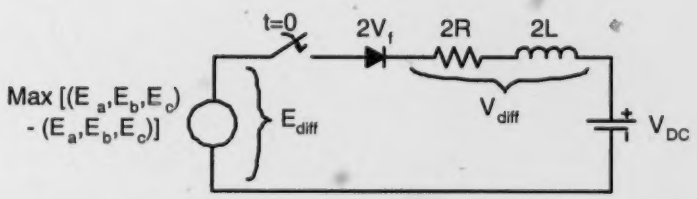

Figure 4.6: Simplified Battery Charging Diagram

$$V_{diff} = 2L\frac{di(t)}{dt} + 2Ri(t) \tag{4.4}$$

The general solution to equation 4.4 is given in equation 4.5 [29].

$$i(t) = K_1 + K_2 e^{-\frac{t}{\tau}} \tag{4.5}$$

In this case, the constants K_1, K_2 and τ can be described by equations 4.6, 4.7 and 4.8.

$$K_1 = \frac{V_{diff}}{2R} \tag{4.6}$$

$$K_2 = i(0) - \frac{V_{diff}}{2R} \tag{4.7}$$

$$\tau = \frac{L}{R} \tag{4.8}$$

$i(0)$ is the current from the previous simulation cycle and t the time difference between the cycles.

When simulating over very long time frames (ie. 100 seconds or more), the number of data points required by the Nyquist theorem became prohibitively large. Therefore, the maximum number of data points was limited to a reasonable value and the results were filtered to create smooth curves.

4.3.2 Simulated Ideal Relationship

The simulation algorithm takes into account more non-ideal effects than the calculation described in section . Therefore, to develop a linear control relationship between electrical frequency and DC voltage, the simulation was incrementally stepped through multiple wind speeds while the DC voltage was varied. The DC voltage and corresponding electrical frequencies that gave the highest output power were subsequently recorded.

The resulting relationship is shown in figure 4.7 with two dotted lines superimposed. Line 1 is the relationship that the controller will attempt to follow and can be described as

$$V_{DC} = 0.114\omega_e + 10. \tag{4.9}$$

This line effectively follows the ideal relationship for most wind speeds of significant power. That is, wind speeds above 5 m/s, where the electrical frequency is,

$$\omega_e = 4\omega_m = 4\frac{TSRv_w}{r} = 4\frac{(7.5)(5m/s)}{1.0m} = 150rad/s. \tag{4.10}$$

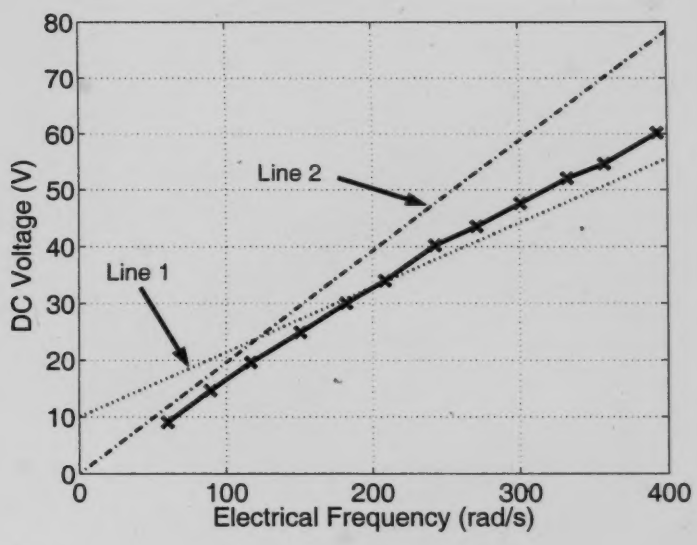

Figure 4.7: Simulated Ideal Relationship

Below 150 rad/s, the DC link voltage is tied to the generator induced voltage limit and will follow line 2. In this way, the relationship between electrical frequency and DC link voltage will actually follow two lines to closely approximate the ideal relationship. It is important to note that the effect below 150 rad/s highlighted by line 2 would not happen in a system without a controlled DC link voltage. In a system without control, the DC link voltage would remain fixed. However, in the system with control, the DC-DC converter allows the DC voltage to follow the generator voltage limit.

4.3.3 Dynamic Simulation Results

A variable wind speed profile was now applied to the simulation and the system was controlled to follow the fixed relationship between electrical frequency and DC link voltage. These simulations were compared against the situation where the DC link is at a fixed voltage.

Simulation With a Fixed DC Link

Initially, the system was simulated using a fixed DC link voltage of 36 volts. Figure 4.8 displays the results for DC voltage, RPM, TSR and DC power. The wind speed followed a profile that can be described by

$$v_w = \mid 8sin(\frac{t}{36}) + 0.8sin(\frac{t}{4}) \mid \ +2. \tag{4.11}$$

In this simulation, the turbine rarely operates at its ideal TSR value of 7.5 and as

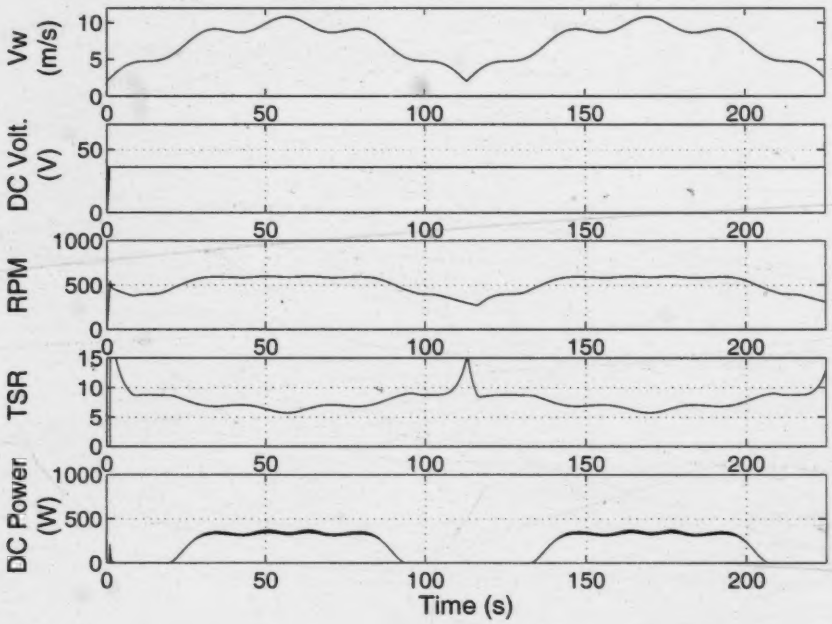

Figure 4.8: Simulation Results With a Fixed DC link Voltage of 36 V

the wind speed varies, the generator speed change is relatively small. The generator is attempting to match the generated voltage with the constant voltage on the DC link. When the wind speed is above 5 m/s, the generator attempts to speed up, but as it speeds up, the internal generated voltage increases. Since the voltage on the generator terminals is fixed, the generator current must also increase. From equation 4.12,

$$T = K\phi I \tag{4.12}$$

a torque is produced that limits the generator speed. When the wind speed is low, the generator terminal voltage is higher than the DC link voltage. Therefore, there is no

current flow out of the generator, the torque is zero and the changes to the generator speed are small. As a result, below a wind speed of 5 m/s, the power capture is zero.

Simulation With Proposed Control

When the simulation was changed to use the proposed control, system performance improved significantly. Notice in figure 4.9 that the TSR stays much closer to the ideal and that the RPM is always changing with wind speed. In the low wind speeds, the power capture is significantly higher. This is an important result considering the fact that low wind speeds are very common. Clearly, the system with the proposed control will, over time, capture more power than a system with a constant DC load.

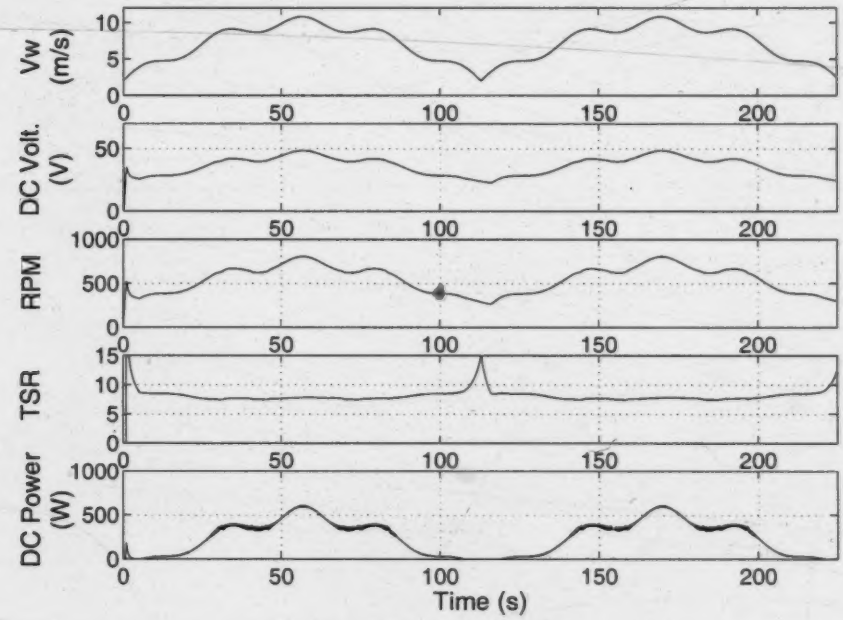

Figure 4.9: Simulation Results With the Proposed Control

The increased power capture is demonstrated in figure 4.10, where the energy and power capture for the simulated time frames are compared.

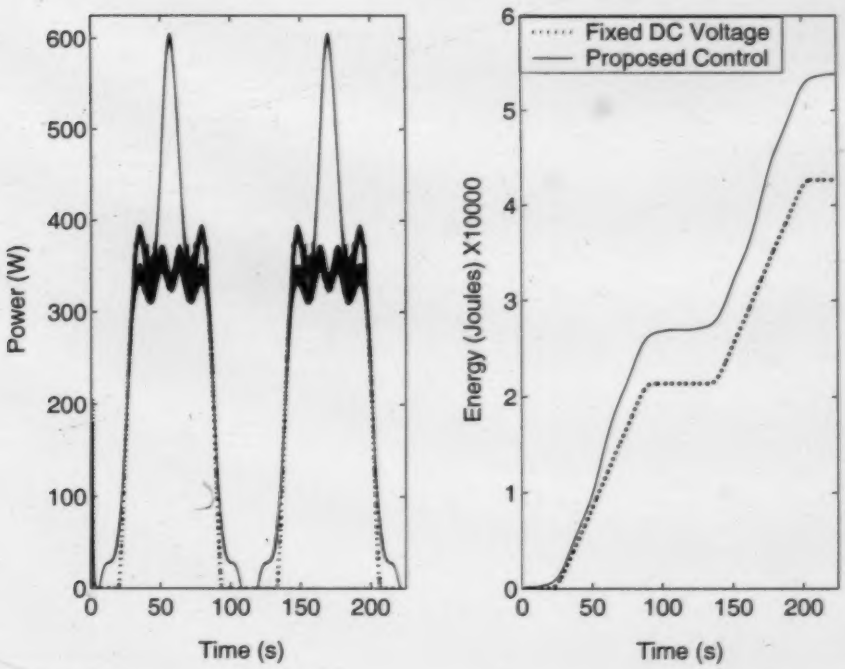

Figure 4.10: Comparison of Simulated Energy and Power Capture

4.3.4 Effect of Changing the DC Offset in the Control Relationship

The control relationship between DC voltage and electrical frequency has a positive DC offset which allows the TSR to operate at just above the ideal value and improves the system response to a step increase in wind speed. To demonstrate the effect of reducing the DC offset, a simulation was run using the following control relationship.

$$V_{DC} = 0.114\omega_e + 8 \tag{4.13}$$

The result is that the system does not respond as quickly to an increasing wind speed (figure 4.11) and, for this wind profile, has a poor power capture. As the wind speed increases, the turbine speed increases as well. However, the increase in turbine speed is so slow that the TSR goes low and the turbine efficiency drops to zero until the turbine catches up to the wind.

If the DC offset is increased above the ideal, then the system response should be good, but the efficiency will be slightly lower. This is seen in Figure 4.12 where the

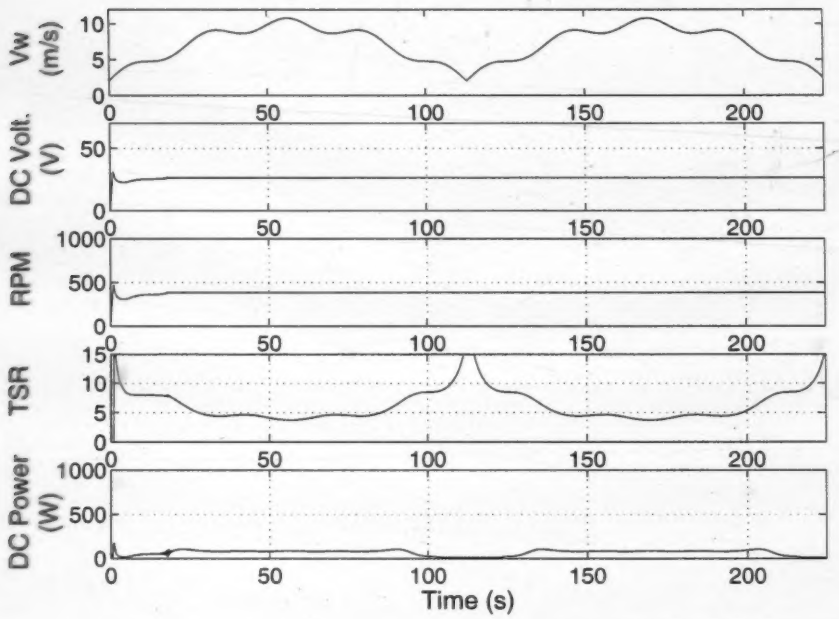

Figure 4.11: Results for a DC Offset of 8 V

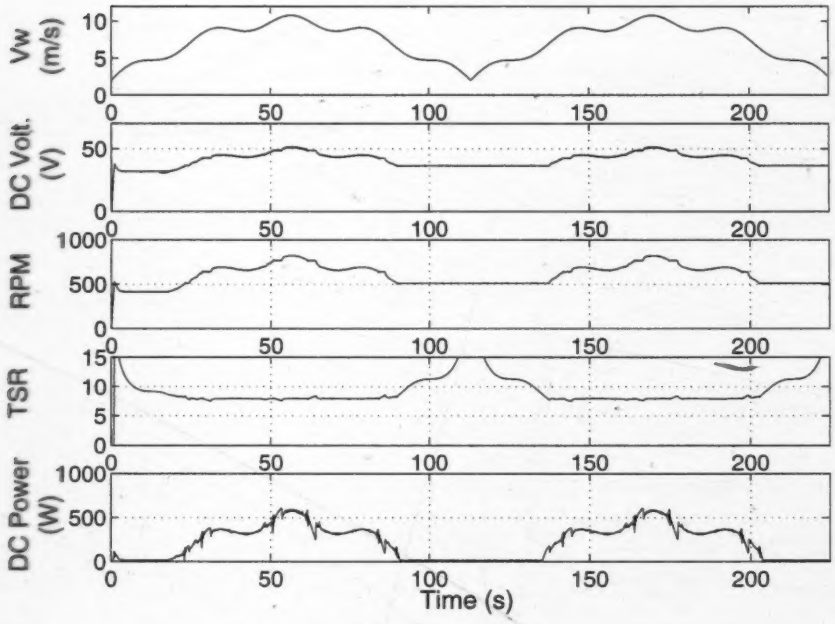

Figure 4.12: Results for a DC Offset of 12 V

DC offset is set to 12 volts. The power capture is slightly lower than in the proposed case, but the turbine gets up to speed more quickly.

These results show that changes in the DC offset can have a significant effect in system performance. A small increase above the best offset will have a marginal impact on system performance, while a decrease will dramatically reduce system performance.

4.4 Fault Detection Circuit Simulation

The purpose of the fault detection circuit is to ensure that the additional power electronics do not compromise the reliability of the original system. The fault detection circuit should sense the switching of a primary boost module, detect if proper switching ceases for a period of time and transfer operation over to a secondary module. Essentially, a basic timing circuit is needed to detect when a switching fault has occurred.

A basic circuit that was designed to accomplish the timing task is seen in Figure 4.13. This circuit is capable of detecting if the switching Mosfet has failed closed.

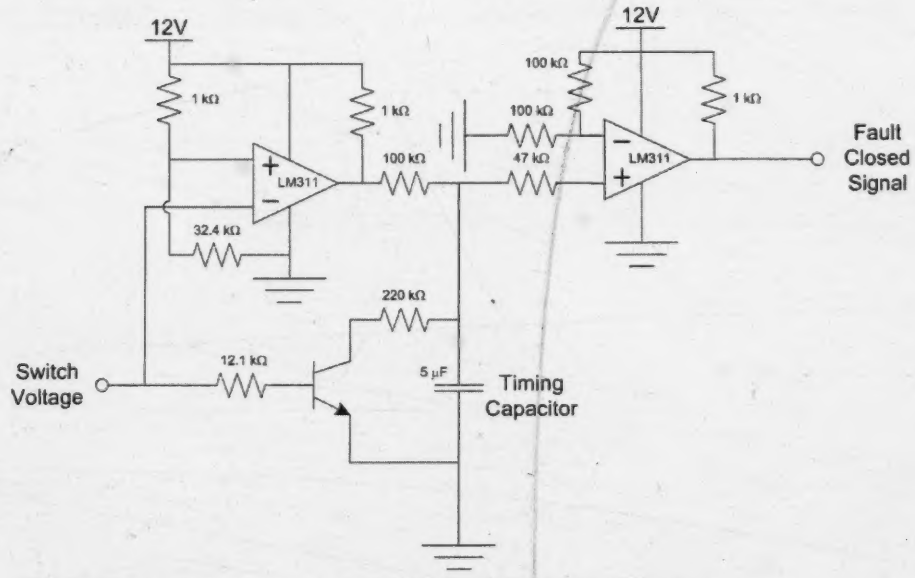

Figure 4.13: "Fault-Closed", Fault Detection Circuit

A second circuit, seen in Figure 4.14 detects a failed open condition. The voltage across the Boost Circuit Mosfet is measured by a digital optocoupler and the output of the optocoupler generates a signal named "Switch Voltage". Switch Voltage will alternate between V_{cc} and ground and as a result, the timing capacitor is repetitively discharged. If the Switch Voltage stays in one state - either at V_{cc} or ground - for too long, the timing capacitor will charge up until the second comparator's threshold is reached and a fault signal is generated.

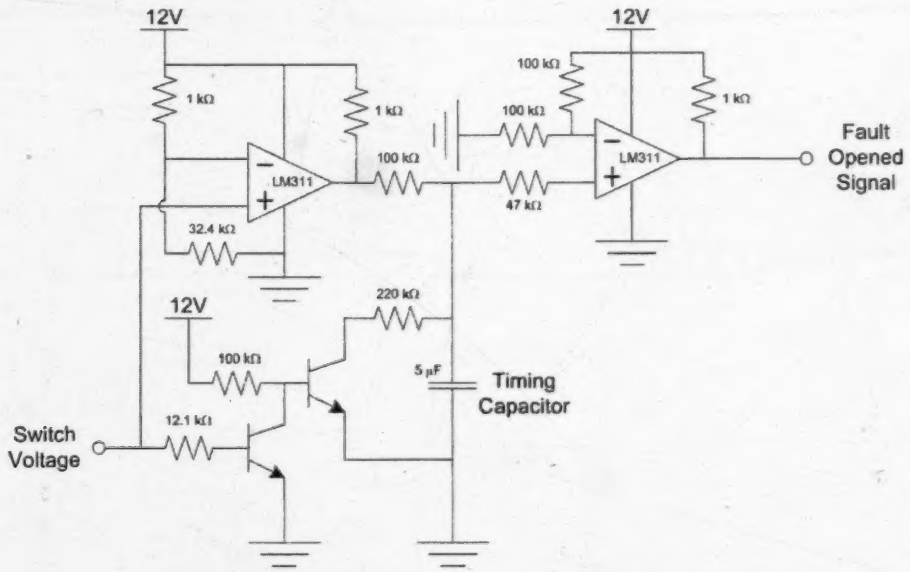

Figure 4.14: "Fault-Opened", Fault Detection Circuit

To verify the operation of these circuits, they were simulated in PSpice. In each of the the "Fault-Opened" and "Fault-Closed" circuits, there are two comparators. The second comparator is solely used to generate an output signal when the capacitor voltage reaches a threshold level. As a result, the simulation did not include these comparators, but included what is shown in figures 4.15 and 4.16. For the circuit in figure 4.15, a square wave switching signal is applied until a time of 0.04 seconds. At 0.04 seconds, the signal goes high, simulating a faulted open condition. The resulting timing capacitor voltage is shown in figure 4.17. Initially, the voltage starts out high, but drops quickly since a proper switching signal is sensed. At time 0.04 seconds, the voltage begins to rise, indicating a fault.

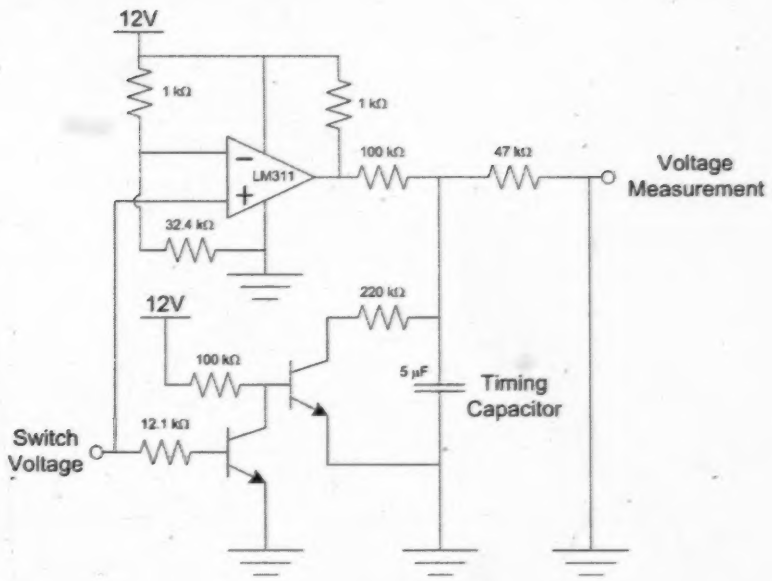

Figure 4.15: "Fault-Opened" Simulation Circuit

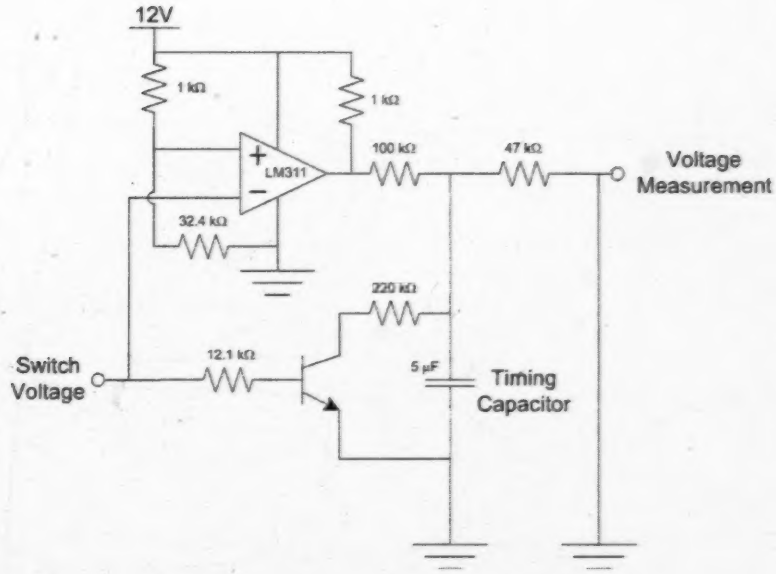

Figure 4.16: "Fault-Closed" Simulation Circuit

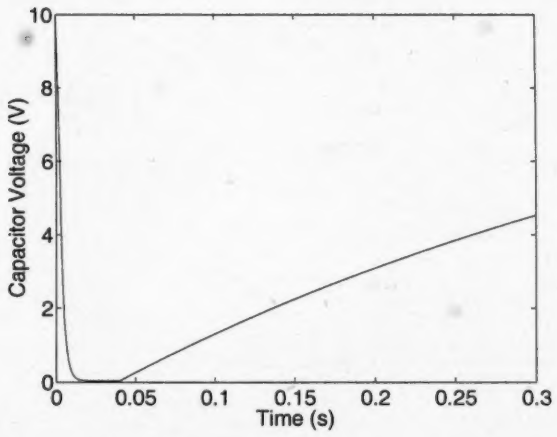

Figure 4.17: "Fault-Opened" Timing Capacitor Voltage

Figure 4.18 is the simulation result for the faulted closed condition. In this circuit (figure 4.16), the timing capacitor voltage is initially low and remains low until a time of 0.04 seconds. At 0.04 seconds, the capacitor voltage begins to grow, indicating a correct detection of the faulted condition. In the final circuit, when this voltage reaches the threshold voltage, a fault signal is generated.

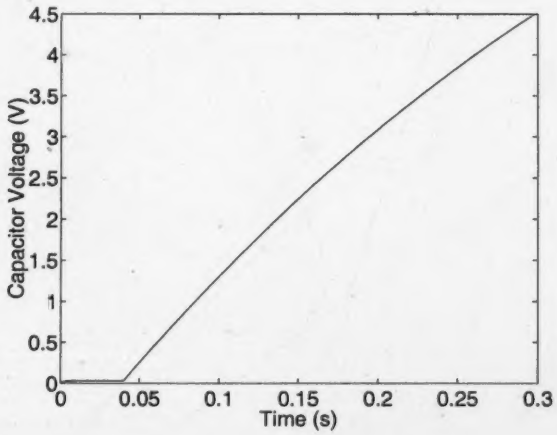

Figure 4.18: "Fault-Closed" Timing Capacitor Voltage

Chapter 5

Experimental Design

The proposed wind energy controller was constructed and verified with the test rig that is illustrated in figure 5.1. A brushless permanent magnet generator is coupled with a DC motor and controlled to model a wind turbine. The output of the brushless permanent magnet generator is fed to the proposed converter, where the electrical power is finally converted to a constant DC output voltage.

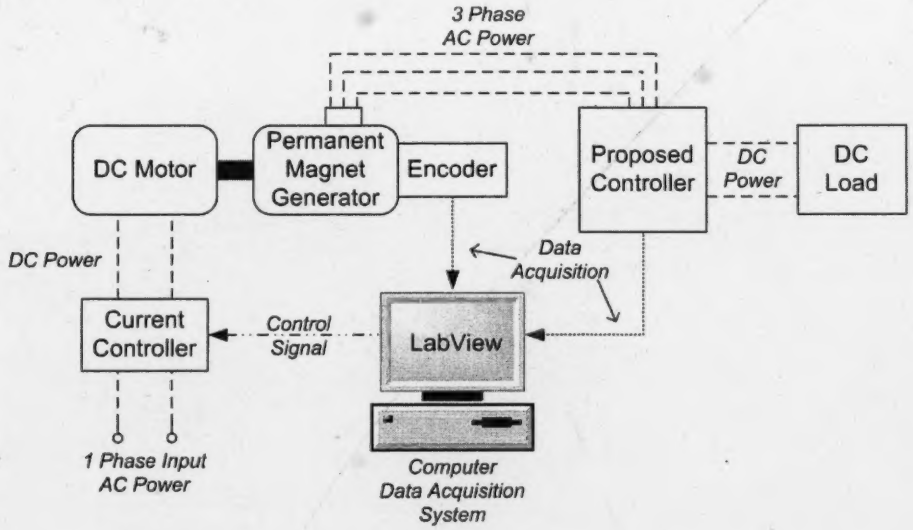

Figure 5.1: Experimental Test Rig Overview

5.1 Wind Turbine Simulator

A wind turbine was simulated with a permanent magnet DC motor, an encoder, a DC current controller and LabView based data acquisition and control. The permanent magnet DC motor was directly coupled to the permanent magnet generator and the wind speed set by a computer controlled input to LabView.

5.1.1 DC Motor

A permanent magnet DC motor was chosen because the current-torque relationship in this type of machine is linear. More explicitly,

$$T = K\phi I, \tag{5.1}$$

and since $K\phi$ (or flux) is fixed in a permanent magnet motor,

$$T \propto I \tag{5.2}$$

The desired turbine torque (or line current) can be set using a computer generated reference voltage and a current controller. The DC motor specifications are given in Table 5.1 and the torque-current relationship is described in Table 5.2.

Table 5.1: DC Machine Specifications

Property	Value
Rotational Speed	1750 rpm
Voltage	180 V_{DC}
Current	14.0 A
Duty	Continuous
Power	3.0 hp

5.1.2 Encoder

The encoder gives an indication of the generator and turbine speeds which are recorded using LabView data acquisition. The speed measurement is used for the turbine simulation and not for the proposed wind energy controller. The encoder gives a square

Table 5.2: DC Motor Torque-Current Relationship

Torque (Nm)	Current (A)
0	0.56
4.75	5.53
11.86	13

wave output that steps between zero and five volts at a frequency of 2000 times the mechanical frequency. It is powered with a five volt supply.

5.1.3 DC Current Controller

Since the DC motor current is linearly related to the DC motor torque, control of the DC current will directly affect the torque. The current control is accomplished with a buck converter, seen in figure 5.2, using a hysteresis current control scheme. The control was implemented with basic analog discrete components. The hysteresis current controller is shown in figure 5.3. The "Current Signal" was measured with a

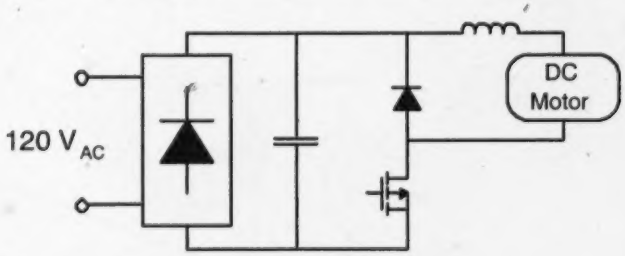

Figure 5.2: DC Current Controller

hall effect sensor which produces an output voltage that is proportional to the current flowing through it. The "Reference" signal is compared to the "Current Signal" and the output switches on and off around a hysteresis band. The output is fed to a digital optocoupler that drives the power mosfet.

The hysteresis band is set by the 100 $k\Omega$ resistor and is centered about the "LEM Signal" input with the 220 $k\Omega$ resistor. According to basic circuit analysis, the circuit in figure 5.3 will have a hysteresis band of about 0.075 volts.

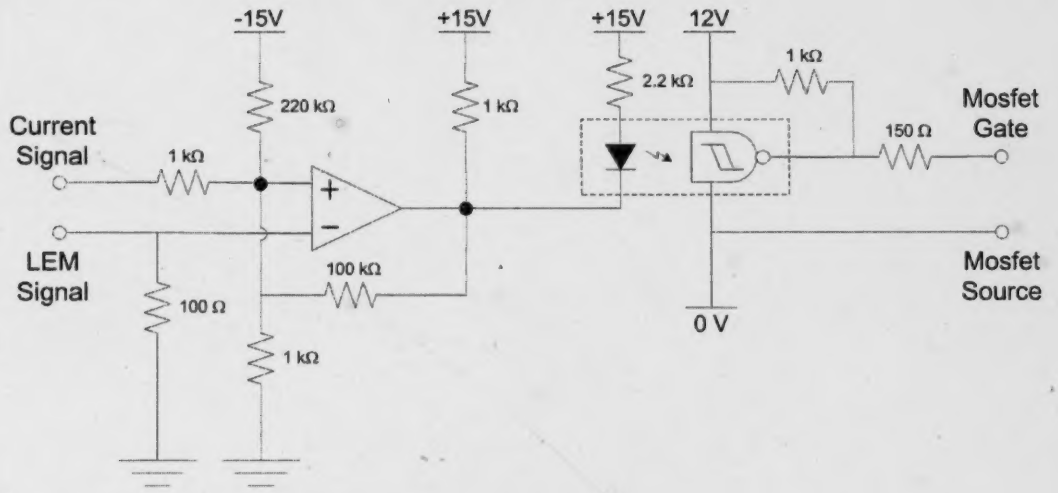

Figure 5.3: Hysteresis Controller

5.1.4 LabView Computer Control

The data acquisition and control was accomplished with a National Instruments DAQ PCI 6024E card and LabView software. The control algorithm is illustrated in figure 5.4.

Based on a wind speed input and the turbine speed measurement (determined from a sample of encoder pulses), the TSR, Cp and turbine torque are calculated. The turbine torque is translated to a desired motor current according to the motor specifications, and then translated to a reference voltage for the current controller. The relationship between reference voltage and motor current is strongly affected by the current sensor's measurement. Therefore, this relationship was accurately determined by experimentally measuring motor currents as the reference voltage was varied.

Since the chosen Cp-TSR curve drops to zero for very low values of TSR, a turbine without an initial speed would not develop any torque to begin moving. To solve this problem, the torque should not be allowed to go below a preset value. When the turbine simulation was actually implemented, the problem of zero was not an issue. The specifications for the DC motor torque-current relationship had a small torque offset to account for friction. The specified offset, however, was slightly higher than

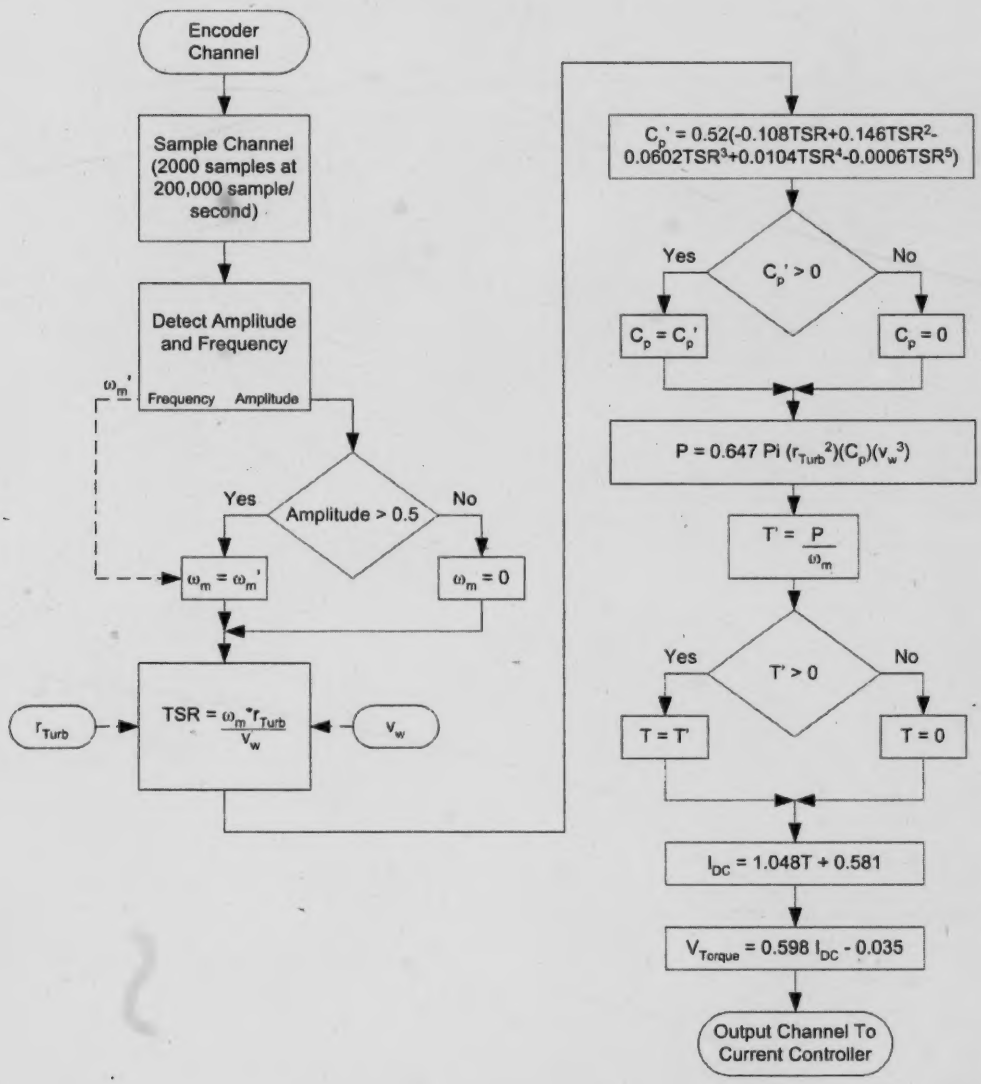

Figure 5.4: DC Motor Control Algorithm

what was actually needed to overcome friction and gave a slight torque value for a command torque of zero.

5.2 Brushless Permanent Magnet Generator

A brushless servo motor was chosen to act as the electric generator. The generator had a high pole number and a high system inertia, making it a good choice for the wind energy test rig. The high pole number allowed for an increase in electrical frequency despite low rotational speeds. The greater inertia helped to create a mechanical system with a slower time response - a characteristic inherent in wind systems. The higher inertia was due to ferrite magnets as opposed to the more commonly used rare earth magnets. The specifications for the brushless permanent magnet generator are given in Table 5.3.

Table 5.3: Brushless Permanent Magnet Generator Specifications

Phase to Phase Winding Inductance	3.71 mH
Phase to Phase Winding Resistance	0.6 Ω
Peak per Phase Torque Constant	0.71 $\frac{Nm}{A}$
Peak Phase to Phase Voltage Constant	86 $\frac{V}{kRPM}$
Maximum Continuous Torque	13 Nm
Poles	8

5.3 DC Load

The converter is being proposed for battery and DC loads. Rather than use actual batteries, which have a finite ability to absorb electrical energy, a system was designed to behave like a battery. The DC load circuit, seen in figure 5.5, is built using a 120 V AC supply, a variac, a diode bridge rectifier, a resistor and a capacitor.

The variac sets the voltage at the input to the diode bridge rectifier, thereby setting the battery, or Boost converter output voltage. This voltage is dropped across the resistor and the voltage ripple is reduced by the capacitor. As the power output from

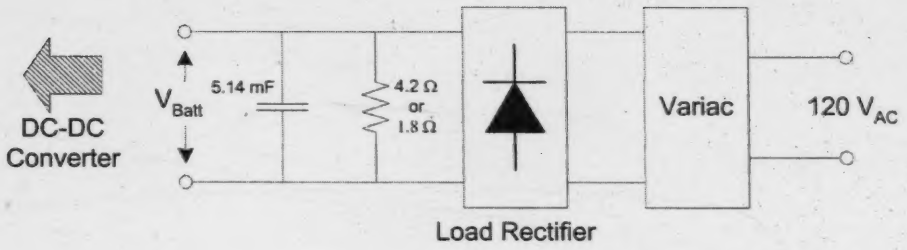

Figure 5.5: DC Load

the wind generator increases, the variac's contribution to the current flowing through the resistor drops. In this way, a battery is modeled which has a semi-stable DC voltage and a resistive current path. The resistance value was changed depending on the desired battery voltage. Since, only two battery voltages were used, only two resistance values were needed; 1.8 Ω was used for a battery voltage of 36 V and 4.2 Ω for a battery voltage of 72 V.

5.4 Proposed Controller

The proposed wind energy controller is composed of four distinct parts: the boost converter, the circuitry to implement the proposed control scheme, the fault detection circuit and the control logic. These four parts are outlined in this section.

5.4.1 Boost Converter

A detailed circuit diagram for the proposed controller is shown in figure 5.6. The generator voltage is rectified to give a variable DC voltage. This is stepped up with the boost converter to a fixed battery voltage which is set by the DC load. The boost converter has a back-up module which can be switched into place by the dual pole relays. The 1 μF capacitors are placed directly across the anode of the diode to the mosfet source for decoupling purposes. The 100 μF capacitors were added because the distance to the DC load was significant and further decoupling was required.

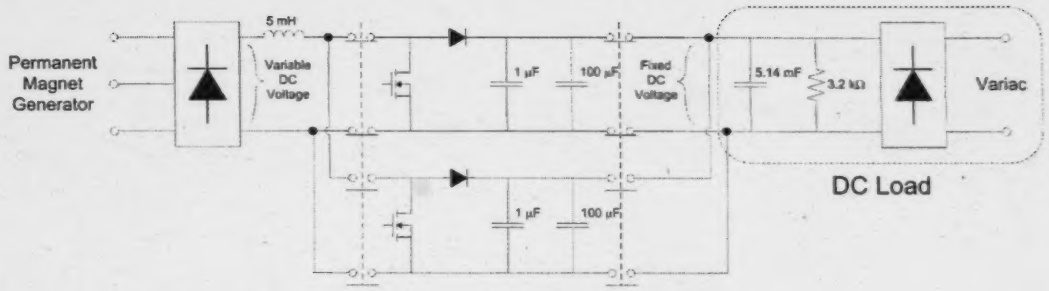

Figure 5.6: Proposed Controller

5.4.2 Circuitry to Implement the Proposed Control Scheme

The linear relationship between electrical frequency and DC link voltage was accomplished with the circuit seen in Figure 5.7. The generator terminal voltage is stepped down by the 115V:25V transformer and applied to a resistor and an anti-parallel diode pair. This provides a small amplitude signal with the same electrical frequency as the generator.

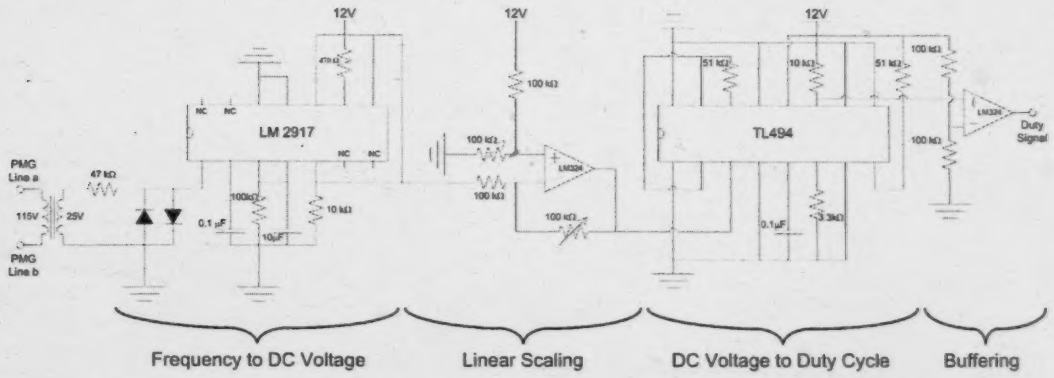

Figure 5.7: Control Scheme Circuit

The frequency of the voltage across the diodes is sensed by the LM2917 - a frequency to voltage converter. The LM2917 generates a DC voltage that is proportional to the frequency. The DC voltage is scaled by an op-amp circuit, establishing the linear relationship between frequency and duty cycle. The output voltage of the op-amp circuit is passed to the PWM circuit (a TL494 integrated circuit), which generates an

output duty cycle based on its input voltage. Finally, the duty cycle signal is buffered with a comparator circuit.

5.4.3 Fault Detection Circuit

The fault detection circuit (figure 5.8) acts upon the Switch Voltage signal, which is an inverted measurement of the power mosfet's drain-source voltage. The circuit is composed of two nearly identical structures - one that detects for an open fault and one that detects for a closed fault. Each structure uses a capacitor for timing, which under normal conditions is repetitively charged and discharged at a rate equal to the duty of the Switch Voltage signal.

For a Fault Closed condition - with a high Switch Voltage - current is supplied to the base of transistor T2, robbing the base current from T1 and turning T1 off. At the same time, comparator C1 is turned on by the high Switch Voltage and begins to charge up Timing Capacitor 1. When the voltage across Timing Capacitor 1 reaches the threshold voltage of 6 volts, a fault signal is generated at the output of C2.

Under a Fault Opened condition, the circuit operates in much the same manner. When the Switch Voltage goes low, transistor T3 turns off and comparator C3 turns on. Timing Capacitor 2 is charged up beyond the 6 volt threshold of comparator C4 and a Fault Signal is generated.

The outputs of both fault detection structures are combined with an OR gate and the result is passed to the output control logic. The $47k\Omega$ resistors are used to isolate the inputs of the second comparators from the outputs of the first comparators. Both the 100 $k\Omega$ and the 47 $k\Omega$ resistors (located between the comparators) affect the charging time of the capacitors.

5.4.4 Control Logic

Figure 5.9 shows the logic that is used to control the switching of the power mosfets and relays. Before reaching the power electronics, the PWM signal and the fault detection signal are combined in the output control logic. The output control logic decides which mosfet should receive the gate signal and when the relays should be turned on. There are several logic inputs which aid in this decision making process.

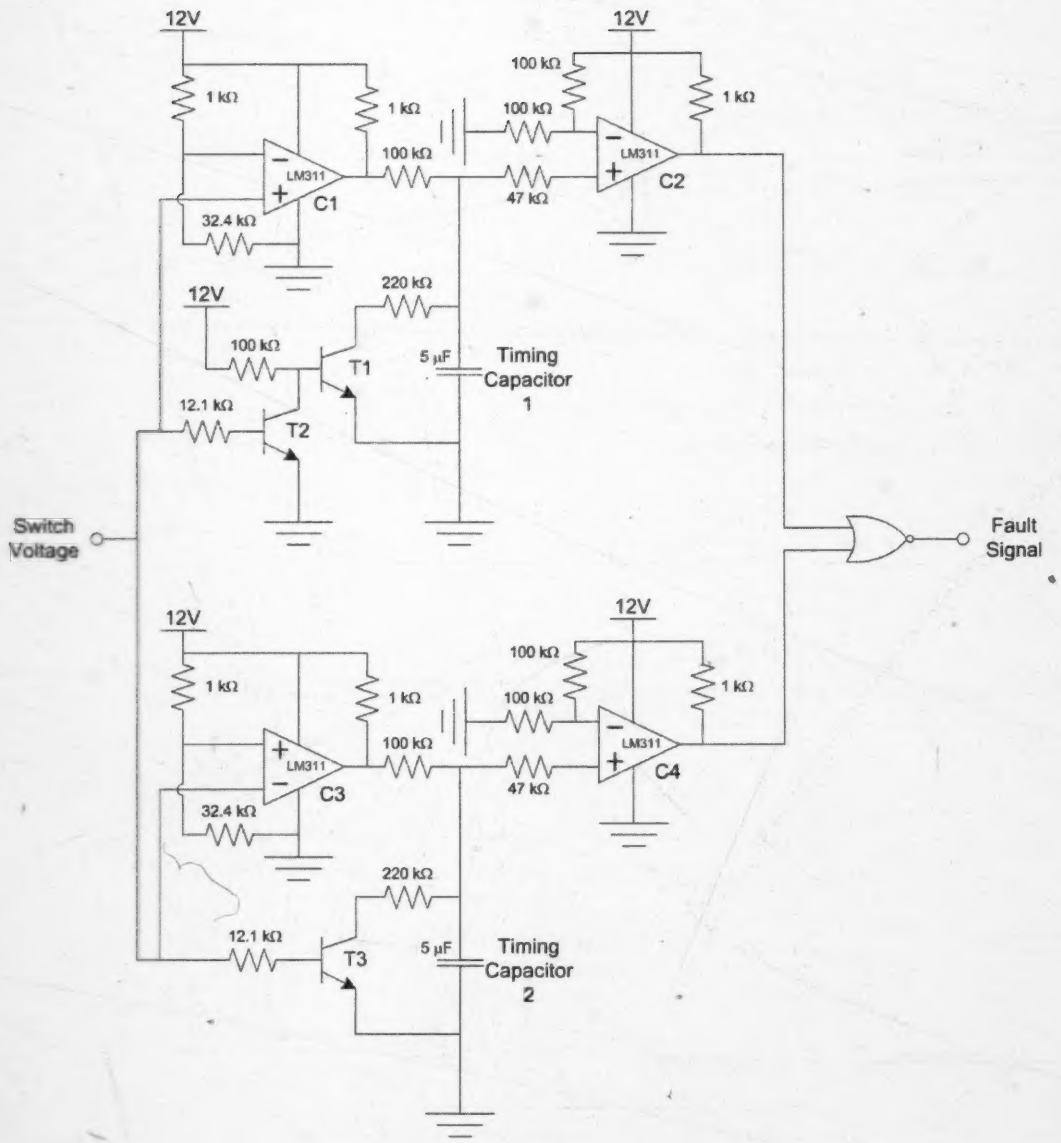

Figure 5.8: Fault Detection Circuit

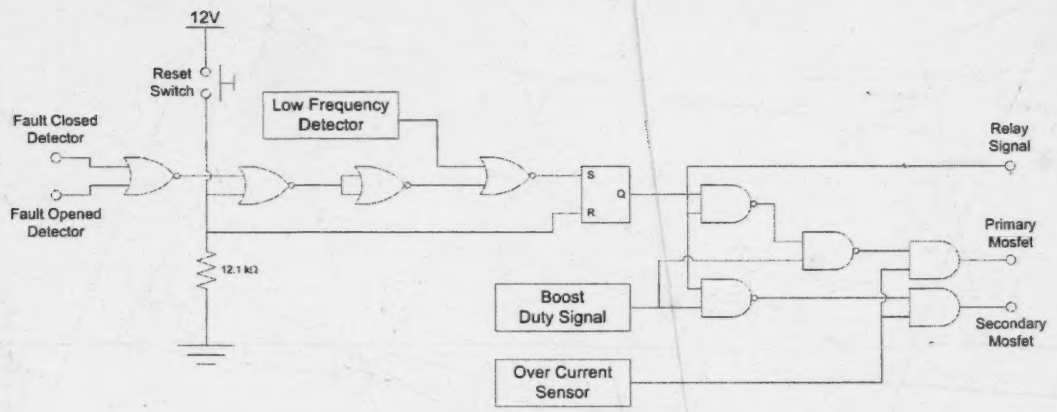

Figure 5.9: Control Logic

Normally, under a fault condition the SR-Latch is set, the relays turn on and the boost circuit signal is changed from the primary to the secondary module. However, once the control has been shifted to the secondary module, there may still be a need for resetting the fault detection circuit. This is accomplished with the reset switch, which upon being pressed, inhibits the "set" signal from the fault detection circuitry and resets the SR latch. The fault detection signal must be inhibited because when the SR latch is set, the primary mosfet does not receive a gate signal. Therefore, the fault detection circuit sees the primary gate as faulted and continuously generates a "set" signal.

If the wind turbine is turning very slowly, the generator output voltage will be very low, making the voltage on the DC link low as well. The optocoupler, which measures the drain-source mosfet voltage, has a digital input and could see this as a faulted closed condition. Therefore, the Low Frequency detector was included to prevent this from happening.

To protect against an over-current, the current through the DC link is measured and compared to a reference value. If it did rise too high, the "over current" signal would go low and inhibit the power mosfet from being turned on.

5.5 Summary

This chapter describes the experimental setup used to evaluate the proposed controller. The structure of the proposed controller is also presented. Chapter 6 presents the experimental results.

Chapter 6

Experimental Results

The experimental results are divided into two main components. First, the control algorithm is verified with test results showing steady state and dynamic performance. Secondly, the fault detection scheme is verified by inducing a fault in the system.

6.1 Control Scheme

The proposed control scheme was experimentally verified by first determining the ideal steady state operating conditions. Based on the ideal conditions, a straight-line control relationship can be deduced and then implemented in a system with a dynamic wind speed.

6.1.1 Verification of the Ideal Relationship

To experimentally determine the straight-line control relationship between electrical frequency and generator terminal voltage, the test rig was stepped through a range of wind speeds. For each wind speed, the duty cycle of the DC-DC converter was independently varied until the ideal TSR was achieved. The resulting relationship between electrical frequency and DC link voltage (shown in figure 6.1) increased nearly linearly with electrical frequency. Superimposed on figure 6.1 is the proposed straight line relationship that will be used in the controller. When compared to the simulated ideal relationship (from section 4.3.2), the experimental ideal relationship proves to have a slightly larger negative concavity for a high electrical frequency

(figure 6.1).

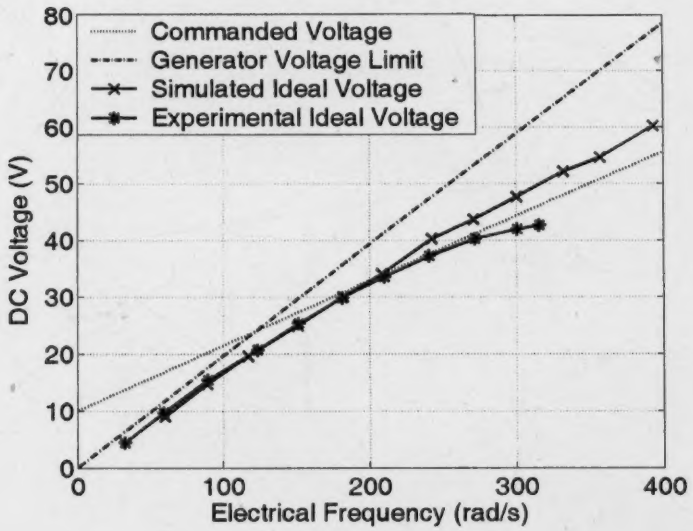

Figure 6.1: Comparison of Optimal Control Relationships

Under these ideal steady state conditions, the turbine power and output power would be expected to increase in a cubic relationship with wind speed (equation 2.2) and as can be seen in figure 6.2 the power increases in a cubic relationship with wind speed.

6.1.2 Proposed Control Scheme With a Dynamic Wind Speed

A continuously varying wind speed was applied to the wind turbine simulator in LabView. With the proposed controller set to track the straight-line relationship,

$$V_{DC} = 0.114\omega_e + 10 \tag{6.1}$$

physically measured data (ie. turbine speed, DC link voltage, DC link current, battery voltage and battery current) and computer generated data (ie. time, wind speed, TSR, C_p and turbine power) were recorded to evaluate the performance of the system. The performance of the proposed controller is compared against the performance of a system using a fixed DC link.

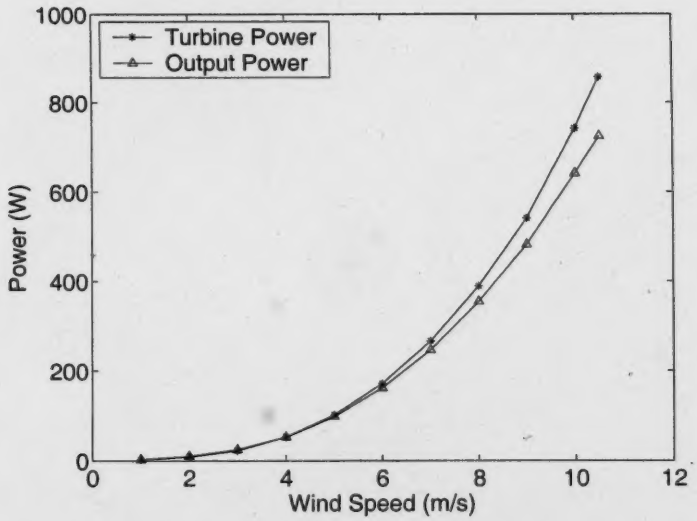

Figure 6.2: Optimal Power Capture

Fixed DC Link

In figure 6.3, the performance of a system using a fixed DC link voltage (ie. figure 2.1) of 36 volts is portrayed. While the power capture in the high wind speeds is good, power capture in the low wind speeds (ie. below 5 m/s) is negligible. The TSR deviates far from the ideal and the RPM hardly changes, indicating that the system is not responding to the changing wind speeds. The poor low wind speed power capture is highlighted in figure 6.4, where power is plotted against wind speed.

The DC link voltage does not stay exactly constant(figure 6.5), but increases with the electrical frequency (figure 6.6). This is due to the way the battery is modeled (figure 5.5). At low wind speeds, the current through the resistor is primarily supplied by the variac. As the current contribution from the generator increases, the current from the variac decreases. Eventually, a point is reached where the DC link voltage exceeds the battery voltage and all the current into the DC load is solely supplied by the generator.

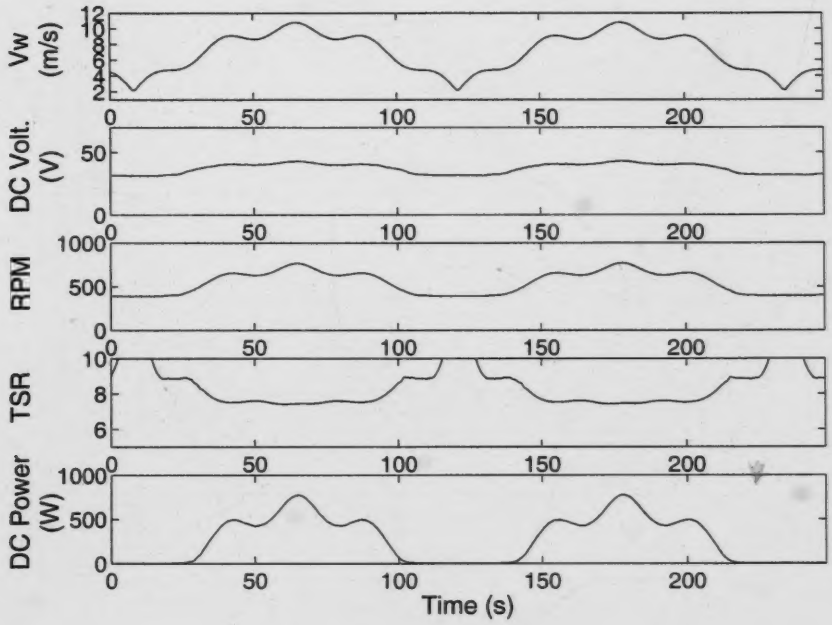

Figure 6.3: Dynamic System Results with a Constant DC Link (36 V)

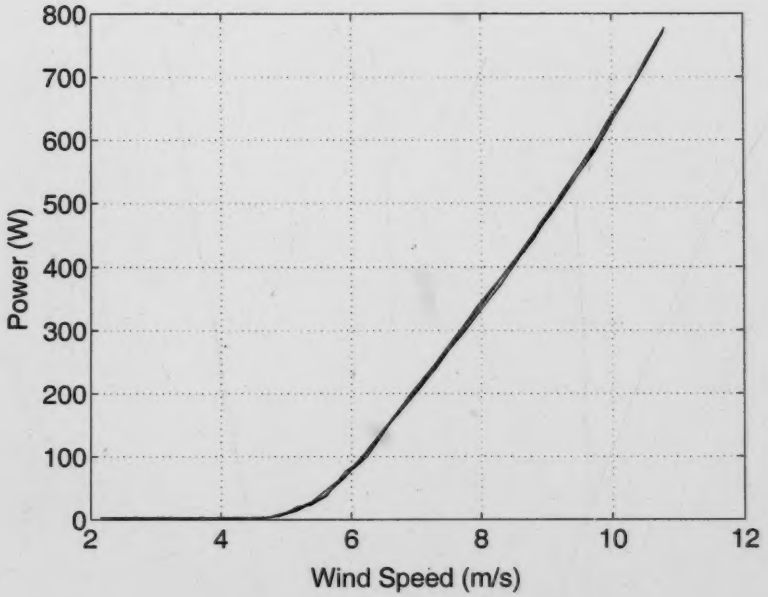

Figure 6.4: Power Capture for a Constant DC Link (36 V)

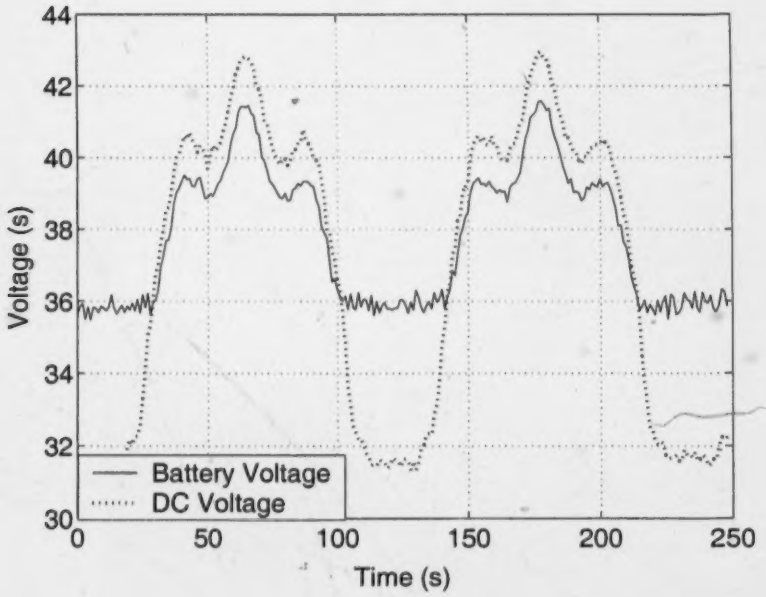

Figure 6.5: DC Link Voltage in the Uncontrolled Case

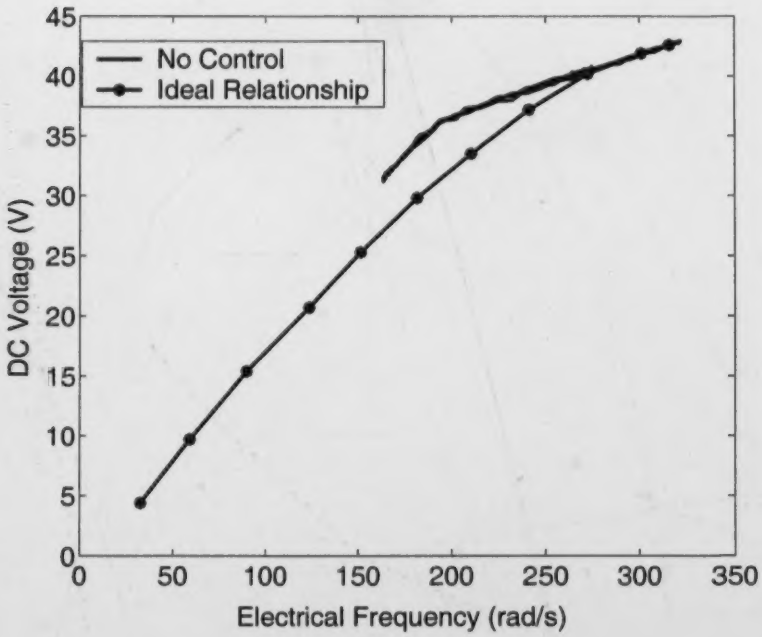

Figure 6.6: Uncontrolled and Ideal DC Link Voltages

In this case, the DC link voltage variation actually aids the high end power capture. This is demonstrated in figure 6.6, where three important areas of operation are implied. First, when the wind speed is low and the generated voltage is not high enough to overcome the reverse bias of the DC link, the generator freewheels at 164 rad/s and the voltage remains fixed at 31.4 volts. Once the wind speed increases above 5 m/s, current is delivered to the load and the DC link voltage begins to rise, closing the gap between the DC link voltage and the "battery voltage." In this region, the variac and generator share the current supply to the DC resistor. Above 194 rad/s, the DC link voltage exceeds the "battery voltage" and all of the current through the DC resistor is supplied by the generator. The DC voltage begins to increase at a lower slope, bringing the battery voltage very close to the ideal. The increases in DC voltage roughly follow the ideal relationship, explaining why the experimental power capture is higher than the simulated.

In a real system that is directly connected to a battery load, the DC link voltage would be expected to rise since every battery load has an internal resistance. However, the slope between DC voltage and electrical frequency will depend on the choice of the battery load. For this case, it is purely coincidental that the DC voltage increases directly to the ideal voltage.

Proposed Control

The proposed control scheme (ie. figure 3.3) improves the power capture dramatically (figure 6.7). The TSR tracks much more closely to the ideal and the RPM changes at every wind speed. The system senses the changing operating conditions and responds to them to improve power capture. The improved power capture is best seen by comparing figures 6.4 and 6.8. More power is captured at every wind speed below 7.5 m/s.

The power capture above a wind speed of 10 m/s is slightly less than the system using the fixed DC link. This may not be a problem since the system is being proposed for low wind speed locations and high wind speed power limiting may be desirable. Furthermore, since batteries have a limited charging rate, it is better to capture some power at all wind speeds rather than lots of power in a region of high wind speeds.

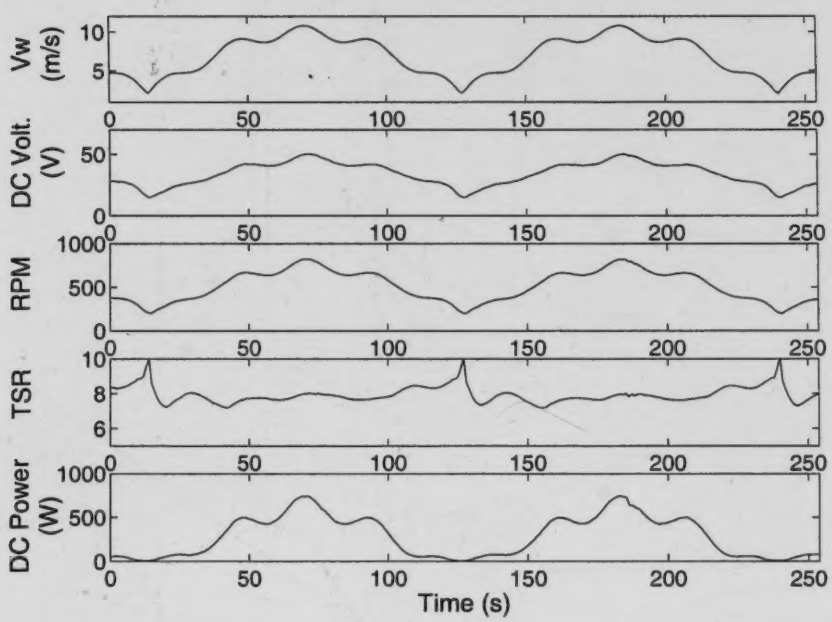

Figure 6.7: Dynamic System Results with the Proposed Control

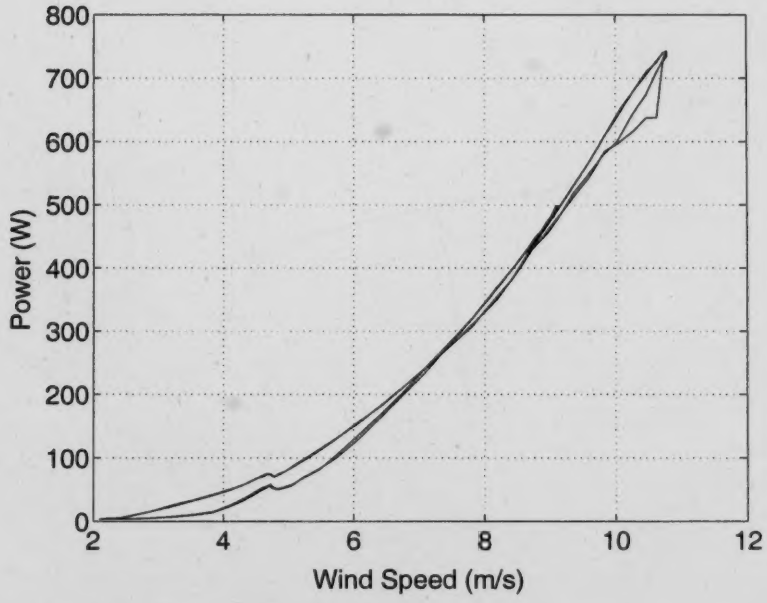

Figure 6.8: Power Capture with the Proposed Control

Improved system performance is also indicated in figure 6.9 where power and energy capture are compared with the system using a fixed DC voltage. Low wind speed power capture is greatly improved and for the chosen wind speed profile, the proposed system captures a greater amount of energy.

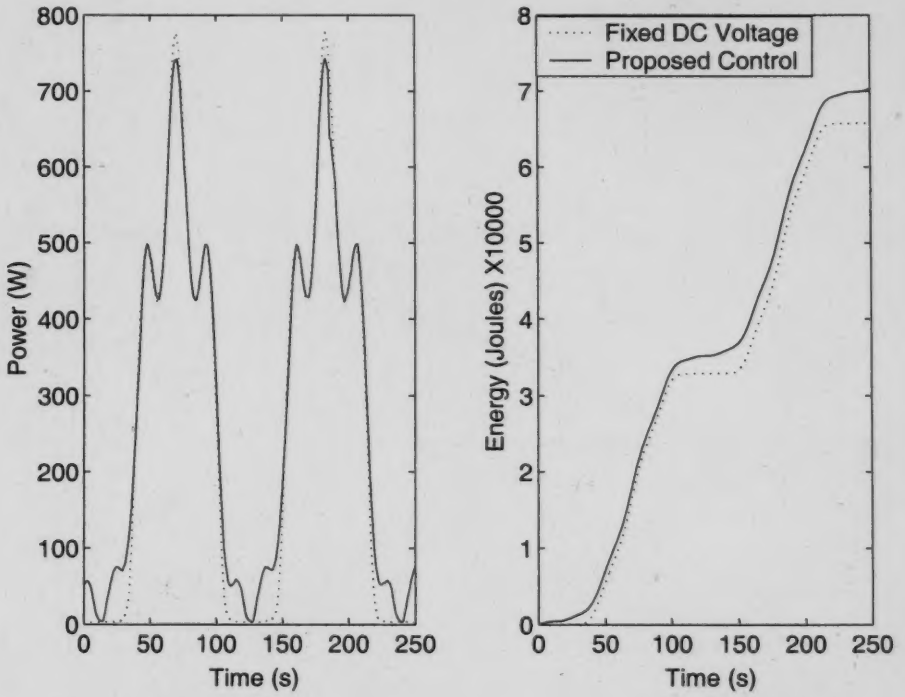

Figure 6.9: Comparison of Experimental Power and Energy Capture

The relationship between electrical frequency and DC voltage, shown in figure 6.10, tracks the control line (line 1) for frequencies above 160 rad/s. Below 160 rad/s, the DC voltage tracks a different line (line 2) that allows for a good power capture in low wind speeds. This knee, which was predicted in figure 4.7, represents an important phenomenon since it allows the system to closely track the ideal relationship with an uncomplicated control scheme.

The knee in the relationship between electrical frequency and DC voltage could be due to two factors: discontinuous conduction of the boost converter or the voltage limit of the generator. To test if knee is due to discontinuous conduction, data for two operating points below the knee was analyzed. Now, the input boundary current

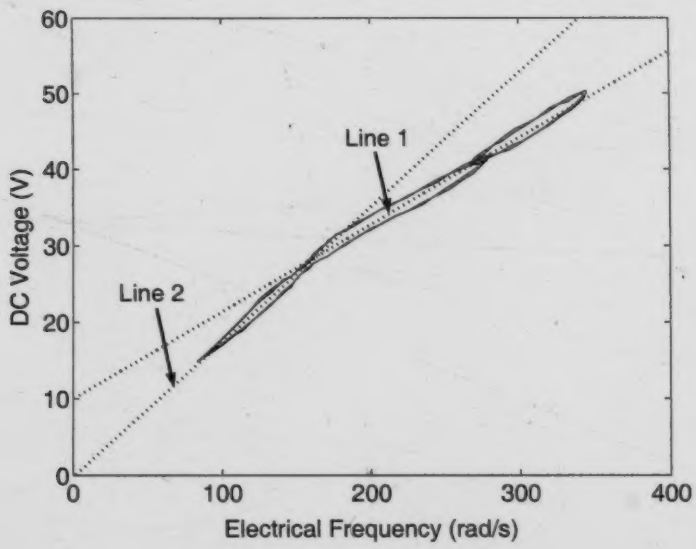

Figure 6.10: Control Relationship

for discontinuous conduction of a boost converter can be described as [30]

$$I_{iB} = \frac{V_o T}{2L}\delta(1-\delta). \tag{6.2}$$

Looking at the plots for the proposed controller, data for two operating points (100 rad/s and 150 rad/s) can be assembled as shown in table 6.1.2. Note that for wind speed, current and power, there are two possible conditions for every electrical frequency. This is due to the differences between an accelerating and decelerating system. If we look at the case where the electrical frequency is 150 rad/s, then the boundary current will be

$$I_{iB} = 0.232A, \tag{6.3}$$

which is less than the observed current of 1.60 A or 2.86 A. Doing the same calculation for 100 rad/s shows that the boundary current is 0.211 A, which is again below the observed current. These results show that discontinuous conduction does not take place and is not the cause for the knee in the measured relationship between electrical frequency and DC voltage. Therefore, the effect of the generator voltage limit must be investigated as the other cause.

Table 6.1: Discontinuous Conduction Calculation Data

	Case 1	Case 2
Elec. Freq.(rad/s)	100	150
Mech. Freq. (rad/s)	25	37.5
Wind Speed (m/s)	2.8 or 3.2	4.45 or 4.75
Output Power (W)	4.5 or 24	43 or 74
Current (A)	0.264 or 1.37	1.60 or 2.86
Generator and Boost Inductance (mH)	8.7	8.7
Commanded DC Voltage (V)	21.4	27.1
Actual DC Voltage (V)	17.5	26.1
Battery Voltage - Ideal (V)	72	72
Switching Frequency (kHz)	4.115	4.115
DC Gain (Commanded)	3.35	2.76
Duty (δ)	0.701	0.638

The generator voltage constant (peak phase to phase volts) is,

$$K_v = 86V/kRPM = 0.821V/rad/s. \tag{6.4}$$

Translating this voltage constant to an ideal bridge rectified voltage gives

$$K_{DC} = 1.35\frac{(0.821V/rad/s)}{\sqrt{2}} = 0.784\ V/rad/s. \tag{6.5}$$

At an electrical frequency of 100 rad/s and 150 rad/s (or 25 rad/s and 37.5 rad/s mechanical), the respective DC voltages (with no losses) will be 19.5 V and 29.4 V. These voltages are just slightly higher than the actual DC voltages, demonstrating that the DC link is following the generator voltage limit. The presence of the boost converter permits the DC voltage to track a voltage that is different from both the commanded relationship and the battery voltage.

6.2 Fault Tolerance Scheme

The fault detection system was tested by removing the primary mosfet's gate signal. When the gate signal was removed, the primary mosfet stayed either open or closed

- depending on which of these states it was in when the gate signal was removed. If the mosfet stayed open, then this looked like a failed open situation. If the mosfet stayed closed, then this looked like a failed closed situation. In either case, the fault detection circuit correctly detected and responded to the faulted condition.

Figure 6.11 shows the response of the system to a switch that fails closed. The first two waveforms are the primary and secondary mosfet gate drive signals. The third waveform is the fault detection signal - the digital optocoupler's measurement of the primary mosfet's drain-source voltage. The fourth waveform is the line-line terminal voltage of the permanent magnet generator.

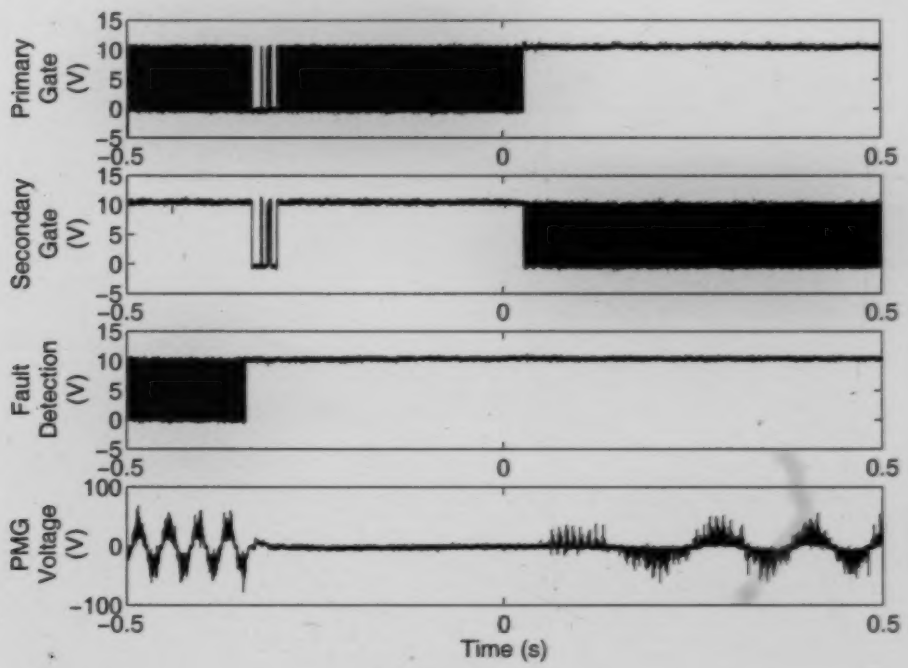

Figure 6.11: Fault Detection Scheme - Faulted Closed

The first event in figure 6.11 is the instant when the primary mosfet stops operating properly. This is seen in the Fault Detection plot. Instead of measuring a continuously switching mosfet, the measurement signal stays positive. Following this, the terminal voltage of the permanent magnet generator drops to zero since the DC link has become a short circuit. The primary gate signal continues to be generated, as is indicated in the first plot, even though the drain to source voltage remains unchanged. The second

event in figure 6.11 is when the switching signal is toggled from the primary gate to the secondary gate. At this point in time the power flow is changed from primary switching module to the secondary switching module and the generator begins to speed up.

Figure 6.12 demonstrates the detection and response to a faulted open switch. Notice that when the gate drive is removed, the generator speed increases and the high frequency noise that was superimposed onto the AC voltage is eliminated. When the gate signal is transferred to the secondary gate, the system resumes normal (ie. pre-fault) operation. It is important to note that for the faulted open results, the turbine simulation was not used and the generator was driven at a fixed torque. The slower time for fault detection, when compared to figure 6.11, is due to a larger timing capacitance. This highlights a convenient feature of the fault detection scheme. The response of the fault detection can be easily modified by changing 2 capacitors.

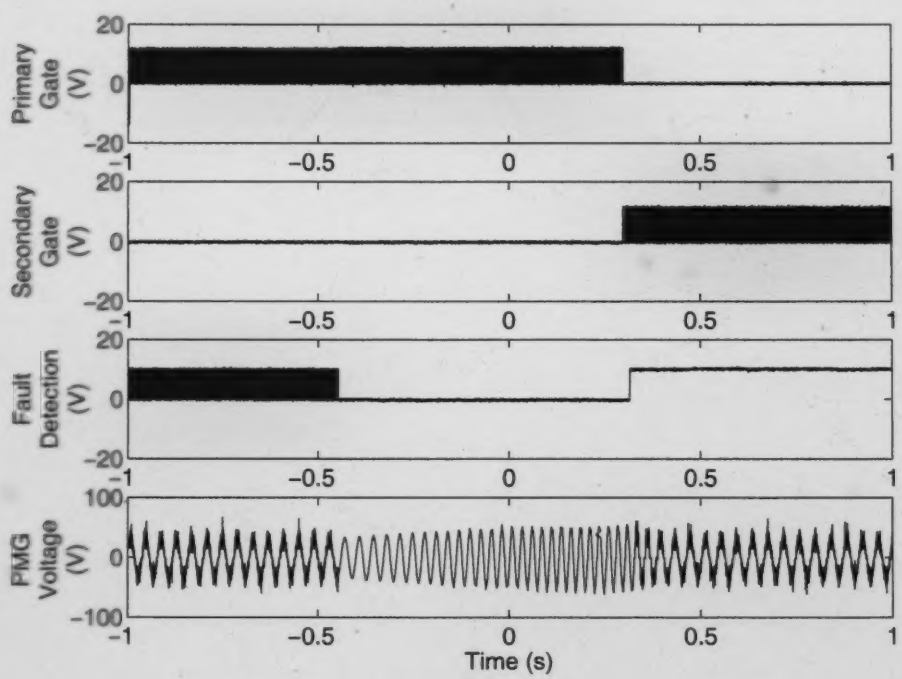

Figure 6.12: Fault Detection Scheme - Faulted Open

Chapter 7

Conclusions and Future Work

The goal of this research was to develop a rugged wind turbine controller for small-scale, stand-alone systems. Small-scale, stand-alone systems are frequently used in conjunction with battery energy storage. A typical design for such systems involves directly connecting the electric generator to a fixed DC link voltage via a diode bridge rectifier. This type of system has been discussed and demonstrated to have unsatisfactory power capture - particularly in low wind speeds. The proposed system uses a DC-DC converter in the DC link to provide electric torque control over the generator. This, in turn, provides control over the operation of the wind turbine.

The DC-DC converter controls the DC link voltage to follow a fixed relationship between generator electrical frequency and DC link voltage. The relationship is a straight line with a postive DC offset. This control scheme provides for three unique areas of operation. When the generator is turning slowly and the induced voltage is below the commanded DC link voltage, the DC link voltage follows the induced voltage. Power flow is enabled in this region where previously no power was captured. When the generator induced voltage exceeds the commanded voltage, the system closely follows the ideal operating conditions. In very high wind speeds, the power capture is restrained because the commanded DC link voltage begins to deviate from the ideal. The proposed control scheme allows for implementation with minimal component overhead, while closely following the ideal operating conditions.

Since the controller is being proposed for stand-alone systems - systems which are located away from major centers - the design ensures that the additional components

do not compromise the existing reliability. As such, the wind turbine controller includes a back up module which can be switched into operation upon failure of the primary module. The switching of the primary module is monitored by fault detection circuitry that can detect for a failed open mosfet or a failed closed mosfet. The DC-DC converter topology was chosen so that minimal components would need to be replaced in case of a fault.

The proposed system was verified in simulation and with a test rig that was designed to model a wind turbine coupled to an AC generator and battery load. Both the control scheme and fault tolerant operation were successfully demonstrated.

The overall design allows for an improved power capture while keeping design complexity to a minimum. The control, which was implemented with discrete analog components, was designed for simple adjustment to accomodate different systems. The fault tolerant scheme improves the reliability of the system (even over a system without a DC-DC converter) by giving indication of a correctly functioning system. If a fault were to occurr, the fault detection signal could be transmitted to a central location. A standard system would not allow for indication of this information.

The proposed controller operated very well in the experimental test rig. The next step would be to test the controller in an real wind turbine and compare the results with an uncontrolled wind turbine. The power capture and reliability of the two systems should be evaluated and compared.

Bibliography

[1] American Wind Energy Association. Wind energy's costs hit new low, position wind as clean solution to energy crisis, trade group says. Wind Energy Fact Sheet, March 6 2001.

[2] BTM Consult ApS. International wind energy development world market update 2001 - record growth! Press Release, April 8 2002.

[3] American Wind Energy Association. Comparative cost of wind and other fuels. Wind Energy Fact Sheet, 2001.

[4] GE Power Systems. GE completes Enron Wind aquistion; Launches GE Wind Energy. Press Release, May 10 2002.

[5] W.D. Kellog, M.H. Nehrir, G. Venkataramanan, and V. Gerez. Generation unit sizing and cost analysis for stand-alone wind, photovoltaic, and hybrid wind/pv systems. *IEEE Transactions on Energy Conversion*, 13(1):70–75, March 1998.

[6] H. Hutchinson. Small-scale power - world-class manufacturers are examining alternatives to the traditional energy market. *Mechanical Engineering*, October 2000.

[7] National Renewable Energy Laboratories. Alaska storm tests turbines. *Wind Power Today*, pages 12–15, 1998.

[8] M. Twidell. Power to the outback (remote-area power generation). *IEE Review*, 34(7):268–269, July 14 1988.

[9] G.L. Johnson. *Wind Energy Systems.* Prentice-Hall, Inc., 1985.

[10] J Hawrelak, T Rachuk, and J Barlishen. *Wind Power in Alberta.* Alberta Research Council Information Series 70, 1976.

[11] R. D. Richardson and G. M. McNerney. Wind energy systems. In *Proceedings of the IEEE*, volume 81, pages 378–389, US Windpower, Livermore, CA, USA, March 1993.

[12] H. Piggot. *Wind Power Workshop.* The Centre for Alternative Technology, 1977.

[13] M.R. Patel. *Wind and Solar Power Systems.* CRC Press LLC, 1999.

[14] E. Muljadi, J. Sallan, M. Sanz, and C.P. Butterfield. Investigation of self-excited generators for wind turbine applications. In *Industry Applications Conference*, volume 1, pages 509–515, Phoenix, Arizona, U.S.A., October 3-7 1999. IEEE.

[15] T. Boutot, L. Chang, and D. Luke. A low speed flywheel system for wind energy conversion. In *IEEE Canadian Conference on Electrical and Computer Engineering*, volume 1, pages 251–256, Winnipeg, Manitoba, May 12-15 2002. IEEE.

[16] R.W. Creighton and J. Ilow. Load commutation for stand alone wind and pv hydrogen energy system. In *2000 Canadian Conference on Electrical and Computer Engineering*, volume 1, pages 555–558, Halifax, Nova Scotia, March 7-10 2000. IEEE.

[17] E. Muljadi, L. Flowers, J. Green, and M. Bergey. Electric design of wind-electric water pumping systems. *Journal of Solar Engineering, Transactions of the ASME*, 118:246–252, 1996.

[18] P. Gardner. Wind generator and drive systems. *Wind Directions, Magazine of the European Wind Energy Association*, pages 16–18, October 1997.

[19] E. Muljadi, K. Pierce, and P. Migloire. A conservative control strategy for variable-speed stall-regulated wind turbines. In *19th American Society of Mechanical Engineers (ASME) Wind Energy Symposium.* ASME, January 10-13 2000.

[20] S. Muller, M. Deicke, and Rik W. De Doncker. Doubly fed induction generation system for wind turbines. *IEEE Industry Applications Magazine*, May/June 2002.

[21] S. Drouilhet, Muljadi, Holz, and R. Gevorgian. Optimizing small wind turbine performance in battery charging applications. In *Wind Power'95*, pages 403–413, Washington D.C., March 27-30 1995.

[22] G. Venkataramanan, B. Milkovska, V. Gerez, and Nehrir H. Variable speed operation of permanent magnet alternator wind turbines using a single switch power converter. In *Journal of Solar Engineering, Transactions of the ASME*, volume 118, pages 235–238, November 1996.

[23] N. Yamamura, M. Ishida, and T. Hori. A simple wind power generating system with permanent magnet type synchronous generator. In *IEEE 1999 Conference on Power Electronics and Drive Systems*, volume 2, pages 849–854, Hong Kong, July 27-29 1999.

[24] G.L. Bianco, O. Honorati, and F. Mezzetti. Small-size stand alone wind energy conversion system for battery-charging. In *Proceedings of the 31st Universities Power Engineering Conference*, volume 1, pages 62–65, September 1996.

[25] W. Lawrance, D. Langridge, and D. Johnston. Low wind generation scheme. In *Renewable Energy*, volume 4, pages 489–494, 1994.

[26] A.M. De Broe, S. Drouilhet, and V. Gevorgian. A peak power tracker for small wind turbines in battery charging applications. *IEEE Transactions on Energy Conversion*, 14(4):1630–1635, December 1999.

[27] I. Schiemenz and M. Stiebler. Control of a permanent magnet synchronous generator used in a variable speed wind energy system. In *IEEE International Electric Machines and Drives Conference*, pages 872–878, Cambridge, Massachusetts, June 17-20 2001. IEEE.

[28] S. Bowmick and R. Spee. Wind speed estimation based variable speed wind power generation. In *Proceedings of the 24th Annual Conference of the IEEE Industrial Electronics Society*, volume 2, pages 596–601, Aug. 31 - Sept. 4 1998.

[29] J.D. Irwin. *Basic Engineering Circuit Analysis.* Prentice-Hall, Inc., Upper Saddle River, New Jersey 07458, 5 edition, 1996.

[30] Dr. John Salmon. *EE 530 Power Electronics.* Electrical Engineering, University of Alberta, 2nd Floor ECERF, Sept. 2000.